Inter-Research Science Publisher

Endangered Species Research
Volume 58:359–379

Published December 4, 2025
https://doi.org/10.3354/esr01456

OPEN ACCESS

North Atlantic right whale *Eubalaena glacialis* summer habitat in the southern Gulf of St. Lawrence, Canada: 2017–2019

Hansen D. Johnson[1,2,6,*], Kimberley T. A. Davies[3], Delphine Durette-Morin[1,4], Meg K. Carr[1], Kimberly J. Franklin[1], Moira W. Brown[4,5], Philip K. Hamilton[5], Amy R. Knowlton[5], Christopher T. Taggart[1,†], Mark F. Baumgartner[2]

[1]Oceanography Department, Dalhousie University, 1355 Oxford St, Halifax, Nova Scotia B3H 4R2, Canada
[2]Biology Department, Woods Hole Oceanographic Institution, 266 Woods Hole Road, MS#33, Woods Hole, MA 02543, USA
[3]Department of Biological Sciences, University of New Brunswick, 100 Tucker Park Rd, Saint John, New Brunswick E2L 4L5, Canada
[4]Canadian Whale Institute, 16 Herring Cove Road, Welshpool, New Brunswick E5E 1B6, Canada
[5]Kraus Marine Mammal Conservation Program, Anderson Cabot Center for Ocean Life, New England Aquarium, Central Wharf, Boston, MA 02110, USA
[6]*Present address:* Kraus Marine Mammal Conservation Program, Anderson Cabot Center for Ocean Life, New England Aquarium, Central Wharf, Boston, MA 02110, USA

ABSTRACT: The distribution of North Atlantic right whales (hereafter 'right whales') has shifted since ~2010, as exemplified by the decreased use of several habitats in the Gulf of Maine, lower Bay of Fundy, and Scotian Shelf, and increased occupancy of the southern Gulf of St. Lawrence (sGSL). The goal of this study was to characterize right whale feeding habitat in the sGSL region. We conducted opportunistic oceanographic sampling in the presence and absence of right whales in July and August over 3 yr (2017–2019). Each oceanographic station was typically comprised of a depth-integrated ring net tow and 2 vertical profiles with a conductivity-temperature-depth instrument and optical plankton counter. Of the calanoid copepod taxa, small copepods (e.g. *Centropages* spp., *Pseudocalanus* spp.) were numerically dominant at all stations where data were available, but *Calanus finmarchicus* was also abundant, while *C. hyperboreus* comprised most of the biomass. Net-derived abundance of late-stage *C. hyperboreus* and total biomass were significantly greater at stations where right whales were detected. Logistic regression analysis suggested that a higher probability of right whale detection was associated with a thicker bottom mixed layer and abundant patches of late-stage *C. hyperboreus* near the seafloor. These results offer insights into the vertical distribution and quantity of prey, the quality of the sGSL as a right whale foraging habitat, and the associated implications for right whale recovery.

KEY WORDS: North Atlantic right whale · *Eubalaena glacialis* · Oceanography · Habitat · Gulf of St. Lawrence · *Calanus finmarchicus* · *C. hyperboreus* · Optical plankton counter

1. INTRODUCTION

North Atlantic right whales *Eubalaena glacialis* (hereafter 'right whales') satisfy their energetic demands by ram filter feeding on mesozooplankton (e.g. Watkins & Schevill 1976). Their fine baleen hairs impose a limit on the smallest prey items they can ingest and are thought to have a filtration efficiency similar to a 333 µm mesh plankton net (Mayo et al. 2001). The hydrodynamic drag generated by the large gape and long baleen plates when the whale opens its mouth imposes energetic limits on swimming speed (van der Hoop et al. 2019). While foraging, slow swimming speeds (~1.1 m s^{-1}; van der Hoop et al. 2019) allow

*Corresponding author: hjohnson@neaq.org
†Deceased

Publisher: Inter-Research · www.int-res.com

large, mobile zooplankton to evade capture (e.g. Fleminger & Clutter 1965). This restricts right whale feeding to a relatively narrow size range of zooplankton (nominally 0.5–10 mm; Mayo et al. 2001) compared to what is available in the environment. Because they are optimized for this feeding style, their foraging efficiency depends on external bio-physical oceanographic mechanisms to aggregate these zooplankton into dense, energy-rich patches (e.g. Sorochan et al. 2021b).

Zooplankton sampling in the presence of feeding right whales in numerous habitats in the Great South Channel, lower Bay of Fundy, and Scotian Shelf provides compelling evidence that right whales target superabundant patches (typically in excess of 10^3 copepods m^{-3}) of late-stage (stages IV, V and VI) *Calanus finmarchicus* (e.g. Murison & Gaskin 1989, Beardsley et al. 1996, Woodley & Gaskin 1996, Baumgartner & Mate 2003, Baumgartner et al. 2003a,b, 2017). These zooplankton are likely desirable prey because they contain energy-rich lipid reserves and are highly susceptible to bio-physical aggregation mechanisms, particularly while in a dormant life-history stage known as diapause in which they are thought to behave as neutrally buoyant particles (e.g. Baumgartner & Tarrant 2017, Sorochan et al. 2021b). For example, process studies in the lower Bay of Fundy and Roseway Basin critical right whale habitats (DFO 2017) show that dense, horizontally patchy layers (on the order of 500 m in extent) are formed near the ocean floor via the interaction between copepod behavior and environmental processes or conditions, such as tidal advection, bathymetric constraints, and the bottom mixed layer (Baumgartner et al. 2003b, Michaud & Taggart 2011, Davies et al. 2014).

Despite their apparent proclivity for late-stage *C. finmarchicus*, right whales are capable of feeding on other taxa and target them under certain conditions. For instance, they have been observed feeding on surface patches dominated by smaller calanoid copepods, namely *Pseudocalanus* spp. and *Centropages* spp., in the shallow coastal waters of Cape Cod Bay during winter when late-stage *C. finmarchicus* is seasonally unavailable (Mayo & Marx 1990, Parks et al. 2012). Historical records from commercial whaling off the coast of Scotland suggest that right whales foraged on euphausiids (Collett 1909). Southern right whales *E. australis* have also been observed surface feeding at fast swimming speeds (>3.6 m s^{-1}) on Antarctic krill *Euphausia superba* (Hamner et al. 1988). Additionally, there is anecdotal evidence of right whales feeding near abundant patches of hydrozoans and decapod larvae (Mayo et al. 2001). Right whales likely also target Arctic *Calanus* species, namely *C. glacialis* and *C. hyperboreus* (e.g. Sorochan et al. 2023). These are large, energy-rich copepods that are abundant at higher latitudes within the historical right whale range (Monsarrat et al. 2015) and are preyed upon by bowhead whales *Balaena mysticetus* using a similar foraging mechanism (e.g. Fortune et al. 2020).

The distribution and availability of zooplankton prey often strongly influences the distribution of baleen whales on foraging grounds (e.g. Murison & Gaskin 1989). From 1980 to 2010, right whales were commonly observed foraging in Cape Cod Bay on small copepods during late winter (February–April) and *C. finmarchicus* during early spring (April–May), and in several habitats with abundant *C. finmarchicus* (e.g. the Gulf of Maine, lower Bay of Fundy, Roseway Basin), in the warmer months (June–September; Brown et al. 2007). Right whale distribution in the northeast USA and Canada began to shift around 2010 (Davis et al. 2017, 2019, Record et al. 2019, Meyer-Gutbrod et al. 2021). Occurrence declined in most of the known habitats in the NW Atlantic, with the notable exception of Cape Cod Bay, where occurrence increased (Mayo et al. 2018, Record et al. 2019, Meyer-Gutbrod et al. 2021). Occurrence also increased in a habitat south of Martha's Vineyard and Nantucket that was used historically (Leiter et al. 2017, O'Brien et al. 2022). There is evidence that these shifts broadly coincide with climate-induced changes to ocean circulation that reduced the availability of *C. finmarchicus* in the Gulf of Maine (Record et al. 2019), as well as with anomalously low annual *Calanus* spp. abundance in most regions of the NW Atlantic based on multi-decadal time-series analyses (Sorochan et al. 2019, Meyer-Gutbrod et al. 2022). This reduction in *Calanus* has been linked to low calving rates (Meyer-Gutbrod et al. 2021) and a decline in occurrence on the calving grounds off the southeast USA (Meyer-Gutbrod et al. 2022). The shift in right whale distribution led to increased whale occurrence in regions with unmitigated risks from vessel strike and fishing gear entanglement, such as the southern Gulf of St. Lawrence (sGSL; Davies & Brillant 2019) and the Scotian Shelf (Durette-Morin et al. 2022). The sGSL is presently the only known high occupancy area for right whales in Canadian waters, though sporadic detections occur throughout their known Canadian range (e.g. at least as far north as Newfoundland), with year-round occurrence of an unknown number of individuals acoustically detected on the Scotian Shelf (Durette-Morin et al. 2022). The combined effect of the reduction in calving rates and increased risk of vessel

strike and entanglement mortalities has been proposed as the major barrier to species recovery (Kraus et al. 2005, Meyer-Gutbrod et al. 2021), though these issues are likely complicated by additional stressors, such as the sub-lethal effects of fishing gear entanglement and ocean noise (Rolland et al. 2012, van der Hoop et al. 2017, Moore et al. 2021, Stewart et al. 2021, Knowlton et al. 2022, Stewart et al. 2022).

Right whales have been sporadically observed in the GSL for many years (Brown et al. 2009, Daoust et al. 2017), but their occurrence in the sGSL began to increase substantially in 2015 (Simard et al. 2019, Crowe et al. 2021). The increase in whale abundance combined with risks from vessel strikes and fishing gear entanglements precipitated catastrophic mortality events in 2017 and 2019 in which a total of 21 right whales (~6% of the 2020 population estimate of 336) were found dead in the GSL (Daoust et al. 2017, Bourque et al. 2020, Pettis et al. 2021). The 2017 events initiated unprecedented surveillance and risk mitigation efforts in the region and throughout Atlantic Canadian waters. From 2017 through 2019, nearly the same ~40% of the population, or ~140 individuals, were documented returning to the sGSL each late-spring and summer (Crowe et al. 2021). The majority of whale detections occur in the sGSL, specifically the section of shallow continental shelf (generally <100 m) bounded by the deep Laurentian Channel to the north, Prince Edward Island to the south, the Magdalen Islands to the east and New Brunswick/Quebec to the west (Fig. 1). Right whale detections occur throughout this region, though they tend to concentrate in the western portion (Johnson et al. 2021).

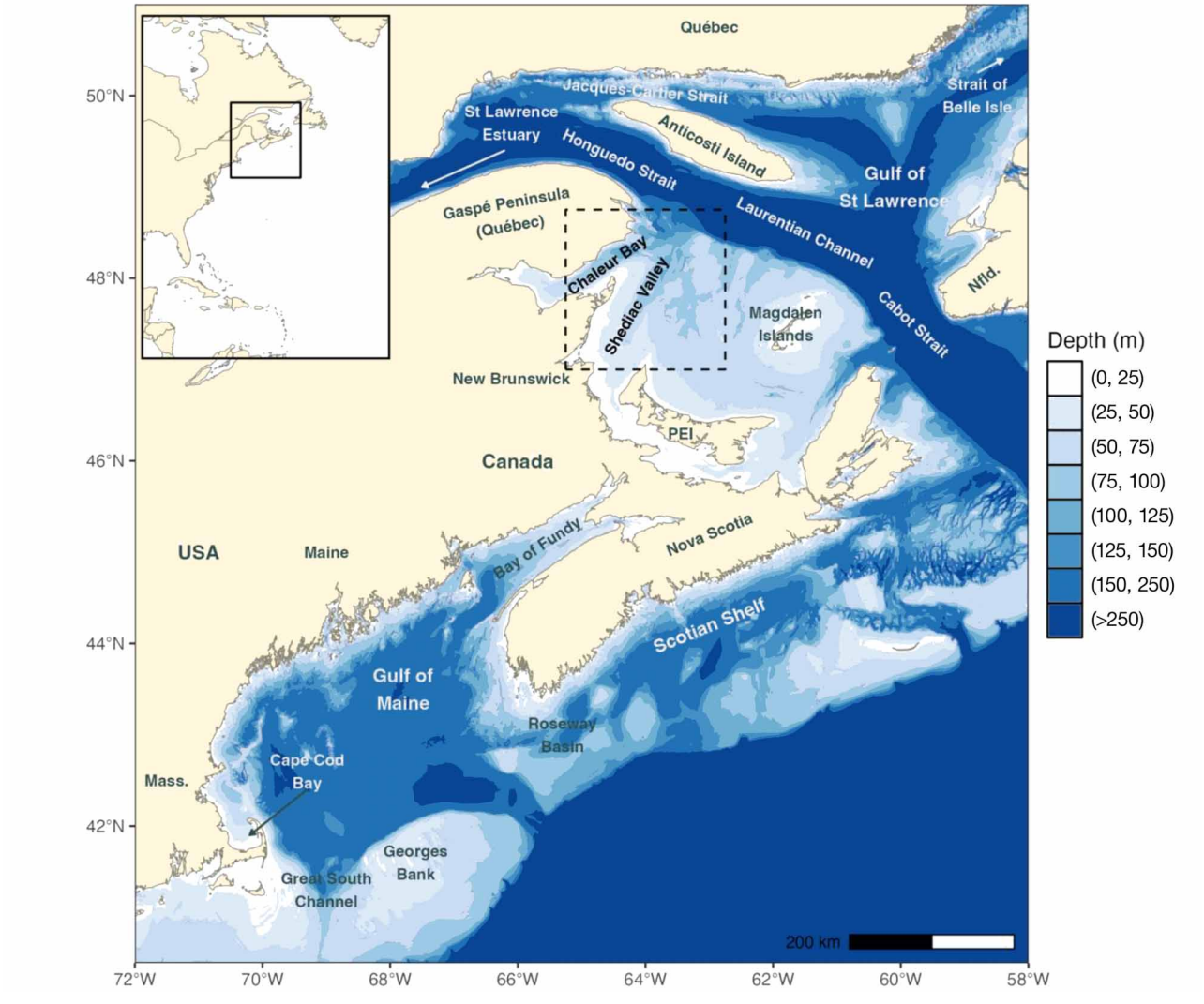

Fig. 1. Study region (dashed line) in the southern Gulf of St. Lawrence, Canada, along with several known right whale habitats (Cape Cod Bay, Great South Channel, lower Bay of Fundy, Roseway Basin) in the northwest Atlantic

Several studies have made efforts to characterize aspects of right whale foraging habitat in the sGSL. Plourde et al. (2019) developed a spatial climatology of *Calanus* spp. (hereafter *Calanus*) in Canadian waters that successfully identified known habitats (e.g. Roseway Basin) and the sGSL as potentially suitable habitats. Sorochan et al. (2019) characterized interannual variation in several regional timeseries of *Calanus* abundance from 1977 through 2016 and discovered negative anomalies in many subregions, including in the sGSL, beginning around 2010. They also found that the average regional abundance in the sGSL was greatest at the Shediac Valley station, in relatively close proximity to the approximate center of the distribution of right whale detections in 2017–2019 (Fig. 1; Johnson et al. 2021). Brennan et al. (2019) combined regional observations with a dynamic transport model to explore mechanisms of *Calanus* transport and supply, as well as to improve estimates of *Calanus* spatial distribution. They found that advection from upstream sources in the western sGSL was likely a major contributor to *Calanus* abundance in the sGSL region. Further extension of this work compared *Calanus* supply in a warm versus cold year, with large differences in late-spring circulation patterns associated with changes in wind forcing that affected *Calanus* supply into the sGSL (Brennan et al. 2021). Gavrilchuk et al. (2021) developed a right whale bioenergetic model that incorporated the *Calanus* climatology by Plourde et al. (2019) to show evidence of highly variable habitat suitability in the sGSL, with generally declining habitat quality since 2014. They suggested that the available biomass in the sGSL was sufficient to support right whale energetic needs in most years but has been decreasing over time, which in turn may contribute to the recent decline in calving rates. A separate, empirical analysis showed evidence of increased reproductive success in the cohort of right whales that are regularly observed in the sGSL relative to those that are not (Bishop et al. 2022), underscoring the uncertainty about the relative quality of the sGSL as a foraging habitat. Most recently, Le Corre et al. (2023) used a 3-D coupled biophysical model to simulate the accumulation of *C. hyperboreus* biomass in different sub-regions of the sGSL in the springtime over a 4 yr period (2016–2019). Their results highlighted the substantial temporal and spatial variability in *C. hyperboreus* biomass in the sGSL and suggested this variability is primarily driven by ocean circulation and the timing of the spring bloom.

All of these habitat studies made use of long-term averaged oceanographic observations to inform their modeling or empirical efforts. While average *Calanus* abundances have been used to attempt to predict right whale presence (e.g. Pendleton et al. 2009), broad-scale background zooplankton sampling does not necessarily reflect prey available to right whales. This is due in large part to the spatial heterogeneity (patchiness) in the distribution of prey and the highly specialized ability of right whales to find these patches in ways that broad-scale sampling cannot (Baumgartner et al. 2007). Furthermore, much of these data were derived from depth-integrated net samples which do not provide information on the vertical distribution of *Calanus*. Right whales are known to target thin, dense layers of *Calanus* (Baumgartner & Mate 2003, Baumgartner et al. 2017), and abundances taken in close proximity to a feeding right whale can be several orders of magnitude greater than those collected in a right whale habitat without whales present (e.g. Baumgartner et al. 2003b).

More recent efforts have made use of finer scale sampling. Sorochan et al. (2021a) quantified spatial variation in copepods in the sGSL using plankton survey data collected in the fall (October) 2018. They documented marked differences in the distribution of *Calanus* spp., with *C. finmarchicus* occurring throughout the region while *C. hyperboreus* and *C. glacialis* were concentrated in the central sGSL. A subsequent study conducted zooplankton sampling in the known right whale habitat in the sGSL in August 2019 (Sorochan et al. 2023). They found evidence of near-bottom aggregations of *Calanus* spp., the biomass of which was typically dominated by *C. hyperboreus* in right whale high-use areas. These studies suggest that a mixed assemblage of late-stage *Calanus* species are likely available to foraging right whales in the sGSL, but these associations have yet to be confirmed or explored in detail using prey data collected in close proximity to right whales. In this study we conducted multi-year oceanographic sampling and visual surveys of right whales in the sGSL to address the following questions: (1) What is the primary prey of right whales in the sGSL, and (2) what are the spatial relationships among right whale presence, prey, and environmental conditions?

2. MATERIALS AND METHODS

2.1. Data collection

2.1.1. Site description

The summertime ocean circulation of the sGSL is dominated by the Gaspé Current, a buoyancy driven,

unstable, coastal jet originating in the St. Lawrence Estuary (Sheng 2001). Upon reaching the tip of the Gaspé peninsula, the eastward flowing current can either remain attached to the coast and turn south into the sGSL, or it can detach from the coast and continue eastward along the southern margin of the Laurentian Channel. These dynamics are primarily influenced by both freshwater runoff from the St. Lawrence Estuary and wind events. In spring (April–June) high runoff combines with highly variable winds, which can alternately favor the coastal attachment or detachment of the Gaspé Current, thus contributing to variations in the southward flow into the sGSL (stronger vs. weaker southward flow, or even reversed, northward flow; Brennan et al. 2021). The summertime water column in the GSL is typically comprised of a surface layer, a cold intermediate layer (CIL) often defined by a temperature of less than 1°C, and a relatively warm, saline deep layer. During the summer months, the CIL reaches the bottom over roughly half of the sGSL region (Galbraith et al. 2020). Tidal currents are relatively small throughout the region (nominally 0.1 m s^{-1}) and increase radially from an amphidromic point west of the Magdalen Islands (Lu et al. 2001). Bathymetry in the sGSL study region is relatively shallow (30–150 m). One of the most notable features is the Shediac Valley, which begins at the Laurentian Channel and shoals southward roughly in parallel with the western coastline of the sGSL (Fig. 1).

2.1.2. Right whale surveys

Oceanographic sampling and visual whale survey efforts were conducted in the sGSL during daylight hours in July and August each year from 2017 through 2019. A 12 m long motor vessel, M/V 'Shelagh I', was used in 2017 and an 18.8 m long snow crab fishing vessel, F/V 'Jean-Denis Martin', was used in 2018 and 2019. The primary objective of each research cruise was to collect photographic identifications (hereafter 'photo-ID') of right whales in the sGSL. Vessel-based right whale photo-ID survey methodology has been developed and refined over more than 40 yr (Brown et al. 2007). Contrary to conventional line-transect sampling, right whale photo-ID surveys did not provide systematic coverage of the survey region. Instead, observers on the survey platform sought aggregations of right whales and attempted to photograph identifiable callosity (e.g. Payne & Dorsey 1983, Kraus et al. 1986) and scarring (e.g. Kraus 1990, Knowlton et al. 2012) patterns of each individual. These photos were submitted to the North Atlantic Right Whale Consortium Catalog (Hamilton et al. 2007) for subsequent analyses, such as mark–recapture population size estimates as well as health and anthropogenic scarring monitoring.

2.1.3. Oceanographic sampling

Oceanographic sampling was conducted on an opportunistic, non-interference basis with the visual surveys and in favorable weather conditions (maximum of Beaufort 5). Sampling was conducted at stations in the morning, mid-day, and evening on each survey day as conditions allowed. The data collected at each station changed slightly after 2017, when we began using a larger vessel with enhanced oceanographic sampling capabilities. In all years, water column depth was determined using the vessel depth sounder.

At each sampling station in 2017, a conductivity-temperature-depth instrument (CTD) cast was used to measure water column conductivity and temperature followed by a vertical net tow to sample the depth-integrated mesozooplankton biomass, abundance, and community composition. The CTD casts were conducted with a Seabird SBE 37 MicroCat programmed to sample at 0.5 Hz. Zooplankton were collected from vertical tows with a 0.75 m diameter ring net with 333 µm mesh size. A depressor weight was fitted to the cod end to maintain the vertical orientation of the net during the tow. A flow meter was positioned off center of the net opening and used to calculate the volume of water filtered. The CTD was also attached in-line with the net above the bridle to record the depth-time series of the haul. A Vemco V16 pressure transmitter was attached to the CTD and monitored from the vessel with a VR100 receiver to measure the depth of the CTD and net in real time without the use of a conductive cable.

Sampling in 2018 and 2019 was expanded to include the use of a profiling optical plankton counter (OPC; Focal Technologies) and a Seabird-19 CTD housed together in an aluminum cage (hereafter a 'cage' profile refers to a combined CTD-OPC profile). Each station comprised a full depth oblique net tow that was immediately preceded and followed by a vertical cage profile. Cage profiles were repeated before and after the net tow in an attempt to resolve spatial variability in zooplankton abundance along the trajectory of the net. The oblique net tows were conducted using a 1 m diameter ring net with 200 µm mesh. A depressor weight was fitted to the net bridle to maintain the horizontal orientation of the net opening during the oblique tow. For all net tows, vertical (2017) or

oblique (2018–2019), efforts were made to achieve a maximum net depth within ~10 m of the sea floor. The cage was lowered vertically through the water column at ~0.5 m s^{-1} to a depth of ~5 m above the sea floor. The same Vemco system from 2017 was used to monitor the depth of the cage and net in real time, as a conductive cable was not available. Either a Seabird SBE 37 or RBR Concerto was attached in-line with the net above the bridle to record the depth–time series of the haul. Net tows were achieved at every station, but the operational limits (maximum sea state of approximately Beaufort 4) for the cage were substantially greater than those of the net (maximum of approximately Beaufort 6), so cage profiles were not conducted at several stations.

2.2. Data processing

2.2.1. Whale detection

The temporal and spatial distribution of right whale observations (i.e. geo-referenced photographs for identification of individual whales) and visual survey effort were used to assess whale detection (detected or undetected) at each oceanographic station. The location of the survey vessel at the time an identification photograph was taken (typically within 200 m of the whale) was used as a proxy for whale position and used to calculate distance to the oceanographic station. Whales were considered detected if at least one right whale was photographed within ±0.5 km of the average position of an oceanographic station and within ±1 h of the initiation of sampling. Whales were considered undetected at a station if survey effort occurred within ±5 km of the station or ±5 h of the initiation of oceanographic sampling and no whales were sighted. These higher minimum thresholds were chosen to increase confidence in whale absence from the area at the time and location of sampling, but it was not possible to confirm absence as whales typically spend much of their time subsurface (e.g. Ceballos et al. 2023), and our survey effort around each station was variable and not systematic. For the stations where whales were undetected, the vessel conducted an average (±SD) of 1.2 ± 0.6 h and 9.6 ± 3.9 km of survey effort within ±5 km of the station and ±5 h of the initiation of oceanographic sampling. Stations at which whales were detected at intermediate temporal or spatial scales (i.e. between 0.5 and 5 km; n = 30) were omitted from subsequent whale detection analyses owing to concerns that sampling was not conducted in sufficient proximity to the whales to accurately resolve the prey field they were targeting. Similarly, stations without associated survey effort (n = 1) were also omitted from whale detection analyses.

These distance and time thresholds for defining whale detection were chosen to compensate for the typical time–space mismatch between visual detections and oceanographic sampling and based on observations of right whale foraging in other habitats. They reflect the finest scale linkages between whales and samples that could be consistently achieved with our study design. Statistical analyses were repeated using several different distance and time thresholds to evaluate the sensitivity of our results to the definition of right whale detection (Text S1 in the Supplement at www.int-res.com/articles/suppl/n058p359_supp.pdf).

2.2.2. Net samples

Zooplankton samples from all tows were rinsed from the net and filtered through a 333 µm sieve. At stations in which sufficient biomass was collected (more than ~50 g wet weight), a subsample (less than ~10% of the total biomass) was randomly selected and immediately frozen in liquid nitrogen for biochemical analysis (results not presented in this paper; see Sobana 2021 and Klymentieva 2022). Taxa abundances were not corrected, as we did not measure species-specific abundance or biomass of the frozen subsamples. The samples (not including the frozen subsample) were preserved in 4% formalin solution buffered with calcium carbonate. After each cruise, individual zooplankton in aliquots of each sample were counted and identified to the lowest possible taxonomic level (usually genus or species) and, for common copepod species, the life cycle stage was also identified by a professional taxonomist (SpryTech). Samples were then filtered and weighed (wet weight) to determine bulk biomass. The total wet weight at which subsamples were taken was corrected by adding the wet weight of an average frozen subsample. Unless otherwise noted, all subsequent zooplankton processing (classification and enumeration) methods were consistent with those used for the Atlantic Zone Monitoring Program (AZMP), which are described in greater detail in Mitchell et al. (2002).

The 128 taxa identified from net samples were later reclassified into 16 groups summarized in Table 1. The grouping of small copepods, early (C1–C3) and late (C4–C6) copepodite stages of *Calanus* spp., krill, amphipods/mysids, and decapods were chosen based

Table 1. Definitions, examples, and summary statistics associated with the 16 groups used to categorize the 128 different zooplankton taxa identified in net samples in the southern Gulf of St. Lawrence. Summary statistics include median abundances across all stations (total; n = 44), stations where whales were detected (n = 20), and stations where whales were not detected (n = 24). Also shown are the test statistics (*W*) and p-values of Mann-Whitney *U*-tests comparing abundance of each group in stations where whales were detected versus undetected. Grey highlighting: significance at $\alpha = 0.05$. NA: not applicable

Group	Definition	Examples	Median abundance (ind. m^{-3})			Mann-Whitney *U*	
			Total	Whales detected	Whales undetected	*W*	p
Amphipods/mysids	Members of the superorder *Peracarida*	*Themisto* spp., *Mysis* spp.	<0.001	<0.001	<0.001	229	0.778
Calanus finmarchicus (early)	Early stage (C1–C3) copepodites	NA	29.8	31.8	21.2	253	0.587
Calanus finmarchicus (late)	Late stage (C4–C6) copepodites	NA	74.4	77.9	72.1	285	0.297
Calanus glacialis (early)	Early stage (C1–C3) copepodites	NA	1.74	1.74	1.28	5	0.4
Calanus glacialis (late)	Late stage (C4–C6) copepodites	NA	4.05	7.1	2.71	38	0.0973
Calanus hyperboreus (early)	Early stage (C1–C3) copepodites	NA	1.92	5.71	1.17	86	0.208
Calanus hyperboreus (late)	Late stage (C4–C6) copepodites	NA	34.7	68.1	25.3	314	0.0412
Cladocerans	Members of the superorder *Cladocera*	*Evadne* spp., *Podon* spp.	8.51	11.1	7.99	280	0.334
Decapods	Members of the order *Decapoda*	*Chionoecetes opilio*, *Homarus americanus*	<0.001	<0.001	<0.001	253	0.707
Fish	Members of the superclass *Pices*	*Gadus* spp., *Urophycis* spp.	<0.001	0.00173	<0.001	269	0.457
Gelatinous	Members of the phyla *Ctenophora* and *Cnidaria*	*Aglantha digitale*, *Cyanea capillata*	<0.001	0.00345	<0.001	302	0.109
Krill	Members of the family *Euphausiidae*	*Thysanoessa* spp., *Mega nyctiphanes norvegica*	16	20.7	14.9	287	0.273
Molluscs	Members of the phylum *Mollusca*	*Limacina* spp.	23.7	25.7	23.3	260	0.654
Non-calanoid copepods	Members of the subclass *Copepoda*, but not of the order *Calanoida*	*Oithona* spp., *Triconia* spp.	677	1270	550	292	0.227
Small calanoid copepods	Members of the order *Calanoida* (excluding *Calanus* spp.)	*Temora* spp., *Centropages* spp., *Pseudocalanus* spp.	259	374	206	256	0.718
Worms	Members of the phyla *Chaetognatha* and *Annelida*	*Parasagitta* spp.	0.332	0.554	0.176	254	0.758

on previous observations of zooplankton taxa near foraging right whales and their apparent food preferences across their range. The other groupings were chosen to combine the remaining taxa into an analytically tractable number of functional groups. Classifications were performed using the World Register of Marine Species (WoRMS; Horton et al. 2021) and the R package *taxize* (Chamberlain & Szöcs 2013). To avoid potential bias from incomplete sampling (e.g. failing to sample close to the bottom), net tows that did not traverse at least 85% of the water column, as inferred from the CTD attached to the net bridle, were excluded from subsequent analyses. We assumed the effects of different net mesh size (333 µm in 2017 vs. 200 µm in 2018/2019) were negligible (e.g. we observed no evidence of clogging in the 200 µm mesh net), especially as all samples were filtered through the same 333 µm sieve immediately after recovering the net in all years. We attempted to account for differences within and between vertical tows (2017; n = 10) and oblique tows (2018/19; n = 34) by normalizing abundance and biomass estimates by the volume of water the net filtered, as determined from the flow meters fitted to each net. Vertical tows filter less water and therefore may underestimate zooplankton abundance, but the influence of this effect on our results was difficult to evaluate given the relatively low numbers of vertical tows and our opportunistic sampling design. Biomasses of late-stage *C. finmarchicus*, *C. hyperboreus* and *C. glacialis* were estimated from net-derived abundances using average individual dry weights previously measured in the region (as in Sorochan et al. 2019). Individual dry weight conversion factors were specific to species, stage, and month (see Table S1.4 in Plourde et al. 2019). Similar estimates were also performed for small copepods using a conversion factor of 13.3 µg ind.$^{-1}$ (Head & Harris 2004). Non-parametric Mann Whitney *U*-tests were used to determine if the median net-derived abundances of each zooplankton group, as well as median net biomass, were different at stations where whales were detected versus not detected. The Mann Whitney *U*-test was used instead of a parametric alternative, such as a Student's *t*-test, because it does not require the underlying data to follow a normal distribution.

2.2.3. CTD

Instrument-specific calibrations were applied to convert raw CTD data into common engineering units of pressure (dbar), temperature (°C) and conductivity (S m^{-1}). The down-cast portion of each CTD profile was manually selected. Outliers were removed using a median filter with a 51-point window. The data were then smoothed by fitting a local polynomial regression (LOESS) curve with a span (alpha) of 0.12. These smoothed down casts were visually compared to the raw data to confirm that only outliers and depth inversions were rejected. Data were averaged in 1 m depth bins. The 2 down casts at each station (before and after the net tow) were averaged to compute a single profile. In rare cases where dedicated CTD or cage profiles could not be conducted, the water column profile was obtained from the CTD attached to the net bridle using the same method described above. As with net tows, CTD casts that did not traverse at least 85% of the water column were excluded from subsequent analyses. The surface mixed layer thickness, a metric indicative of the strength of stratification, was defined as the distance from the surface to the depth of the maximum buoyancy frequency (a measure of vertical water column stability). The bottom mixed layer thickness was defined as the height from the maximum CTD depth to a density change of −0.05 kg m^{-3}, as in Baumgartner et al. (2003b). All oceanographic calculations, including derivation of water column practical salinity (hereafter 'salinity'), potential density (kg m^{-3}; hereafter 'density') and buoyancy frequency (s^{-1}), were computed using the 'oce' package in R (Kelley & Richards 2025).

2.2.4. OPC

OPC data were processed using similar methods as those described by Baumgartner (2003). An analyst reviewed each OPC profile and selected only the down cast for subsequent analysis. Records containing extreme depths, depth inversions, slow descent rates (<0.3 m s^{-1}), or excessive light attenuance (>1800 digital counts) were removed. The volume filtered in each timestep was computed as the area of the OPC tunnel (0.02 m by 0.25 m) multiplied by the change in depth. Profiles of particle abundance (particles m^{-3}) were computed by summing the particles of a given size range in 5 m depth bins and dividing by volume filtered over the same bin interval. A size range of 1.5–5.0 mm equivalent spherical diameter (ESD) was used to represent the abundance of late-stage *Calanus* spp. We chose the lower limit of 1.5 mm based upon work by Baumgartner (2003), who established a predictive relationship between net-derived stage C5 *C. finmarchicus* and 1.5–2.0 mm ESD OPC particle abundance and determined that including smaller size particles led to abundance overestimates.

We expanded the size range to 5.0 mm ESD to account for and incorporate the presence of larger *C. hyperboreus* and *C. glacialis* (Herman, 1992). Owing to considerable overlap in the size ranges of late-stage (C4–C6) *Calanus* species (*C. finmarchicus*: 0.6–2.5 mm ESD, *C. glacialis*: 1.0–3.2 mm ESD, *C. hyperboreus*: 1.3–4.4 mm ESD; Herman 1992), we were unable to use the OPC to determine species- or stage-specific abundances. See Herman (1992) for more information on the relationship between OPC-derived ESD and species- and stage-specific abundances of various taxa. A size range of 0.8–5.0 mm ESD was used for visualization purposes. Depth bins in which the volume filtered was less than 50% of the theoretical volume of the bin (i.e. area of the OPC × 5 m) were rejected. We estimated the wet weight, W_{wet} (mg m^{-3}), of the OPC-filtered particles using:

$$W_{wet} = \frac{3}{4}\pi\left(\frac{ESD}{2}\right)^3 p \quad (1)$$

where ESD is measured by the OPC, and p is the particle density which we assumed was equal to 1 mg mm^{-3} (Suthers et al. 2006, Fortune et al. 2020). Biomass profiles were computed by dividing the sum of the mass of particles in each 5 m depth bin by the volume filtered. OPC casts that did not traverse at least 85% of the water column were excluded from subsequent analyses. All processing was conducted using the 'opcr' package in R (Johnson 2021).

2.2.5. Logistic regression

Several physical and biological variables were derived for each station (Table 2). Bathymetric depth, derived from the vessel depth sounder, was selected because right whales and/or *C. finmarchicus* have been associated with deep basins in the lower Bay of Fundy (Murison & Gaskin 1989, Michaud & Taggart 2011) and Roseway Basin (Baumgartner et al. 2003b, Davies et al. 2013). The SD in the bathymetric depth within a 5 km radius of each station, derived from the GEBCO dataset (accessed from https://download.gebco.net/), was used as a proxy for bathymetric relief, which has been found to play a role in forming *Calanus* aggregations in Roseway Basin (Davies et al. 2013). The water densities at the surface and bottom were chosen to characterize associations with regional water masses, specifically the surface layer, CIL, or deep layer. Surface and bottom mixed layer

Table 2. Results of single-variable logistic regressions of right whale detection a nd a given habitat variable. Sample size (n) varied as not all variables were available at all stations. Coefficient indicates the direction and magnitude of the association; p provides the p-value of a drop-in-deviance test comparing the full and null models. Grey highlighting: significance at $\alpha = 0.05$. GEBCO: general bathymetric chart of the oceans; OPC: optical plankton counter

Variable	Units	Definition	n	Coefficient	p
depth	m	Bottom depth from vessel echosounder	77	5.50×10^{-2}	<0.001
bottom_sd	m	SD in GEBCO bathymetry within 5 km of station	77	-1.20×10^{-2}	0.893
ctd_bottom_density	kg m^{-3}	Water density at max. sampled depth	63	1.94	0.032
ctd_surface_density	kg m^{-3}	Water density at min. sampled depth	63	-1.44×10^{-1}	0.733
ctd_sml_thickness	m	Depth of max. buoyancy frequency	63	-8.30×10^{-2}	0.077
ctd_bml_thickness	m	Height from max. sampled depth to a density change of -0.05 kg m^{-3}	63	2.16×10^{-1}	0.009
net_finmarchicus	ind. m^{-3}	Log-transformed abundance of late-stage (C4–C6) *C. finmarchicus*	45	8.23×10^{-1}	0.246
net_hyperboreus	ind. m^{-3}	Log-transformed abundance of late-stage (C4–C6) *C. hyperboreus*	45	1.03	0.050
net_calanus	ind. m^{-3}	Log-transformed abundance of late-stage (C4–C6) *C. finmarchicus* and *C. hyperboreus*	45	1.09	0.135
net_small_copepod	ind. m^{-3}	Log-transformed abundance of small copepods (defined in Table 1)	45	2.62×10^{-1}	0.533
net_mass	g m^{-3}	Wet weight of net contents	44	1.45	0.041
opc_max	g m^{-3}	Max. OPC biomass	42	1.00×10^{-3}	0.029
opc_avg	g m^{-3}	Average OPC biomass	42	2.00×10^{-3}	0.074
opc_surf_max	g m^{-3}	Max. OPC biomass within 15 m of min. sampled depth	42	0.00	0.830
opc_deep_max	g m^{-3}	Max. OPC biomass within 15 m of max. sampled depth	42	1.00×10^{-3}	0.019

thicknesses were included to evaluate the influence of the vertical structure of the water column. Biological metrics from the net and OPC were used to resolve several aspects of late-stage *Calanus* spp. availability (i.e. vertical biomass distribution; see metric definitions in Table 2). The 1.5–5 mm ESD size class in 5 m depth bins was used for OPC biomass measurements. Zooplankton abundances from net samples were log-transformed prior to logistic regression analysis. Stations from all years and months were combined in a single analysis (i.e. not treated as factors) to maximize sample size (see Table 2 for sample sizes for each regression). Separate, single-variable logistic regressions were fit with each habitat variable as the independent variable and the series of whale detected/undetected scores as the dependent variable to characterize the relationship between each habitat variable and the probability of whale detection. Each model was formulated as follows:

$$\text{logit}(\pi) = \beta_0 + \beta_1 (V) \quad (2)$$

where the logit of the probability of right whale detection, π, is modeled as a linear function of the predictor variable, V, and β_0 is the intercept and β_1 is the model coefficient. The significance of each model was evaluated using drop-in-deviance tests that compared the full model to a null model that lacked the habitat variable of interest, i.e. the term $\beta_1(V)$. Model assumptions (independence of residuals, linearity of predictor variables, absence of multicollinearity, and lack of strong outliers) were assessed and verified graphically.

All analyses were conducted using the R programming language (R Core Team 2020) using the 'oce' (Kelley & Richards 2025), 'shiny' (Chang et al. 2020), and 'tidyverse' (Wickham et al. 2019) packages unless otherwise noted. Visualizations were created using the 'ggplot2' (Wickham 2016), 'ggspatial' (Dunnington 2021), and 'patchwork' (Pedersen 2024) packages.

3. RESULTS

3.1. Sample sizes

Data were collected from a total of 112 stations from 2017 through 2019. Whale detection information was available at 77 stations (36 detected, 41 undetected; shown in Fig. 2). Of the stations with whale detection data, usable CTD profiles were collected from 64 (32 detected, 32 undetected), usable net tows were collected from 44 (20 detected, 24 undetected), and usable OPC profiles were collected from 42 (23 detected, 19 undetected). In total there were 23 stations with whale detection information, as well as usable CTD, net and OPC data (11 detected, 12 undetected).

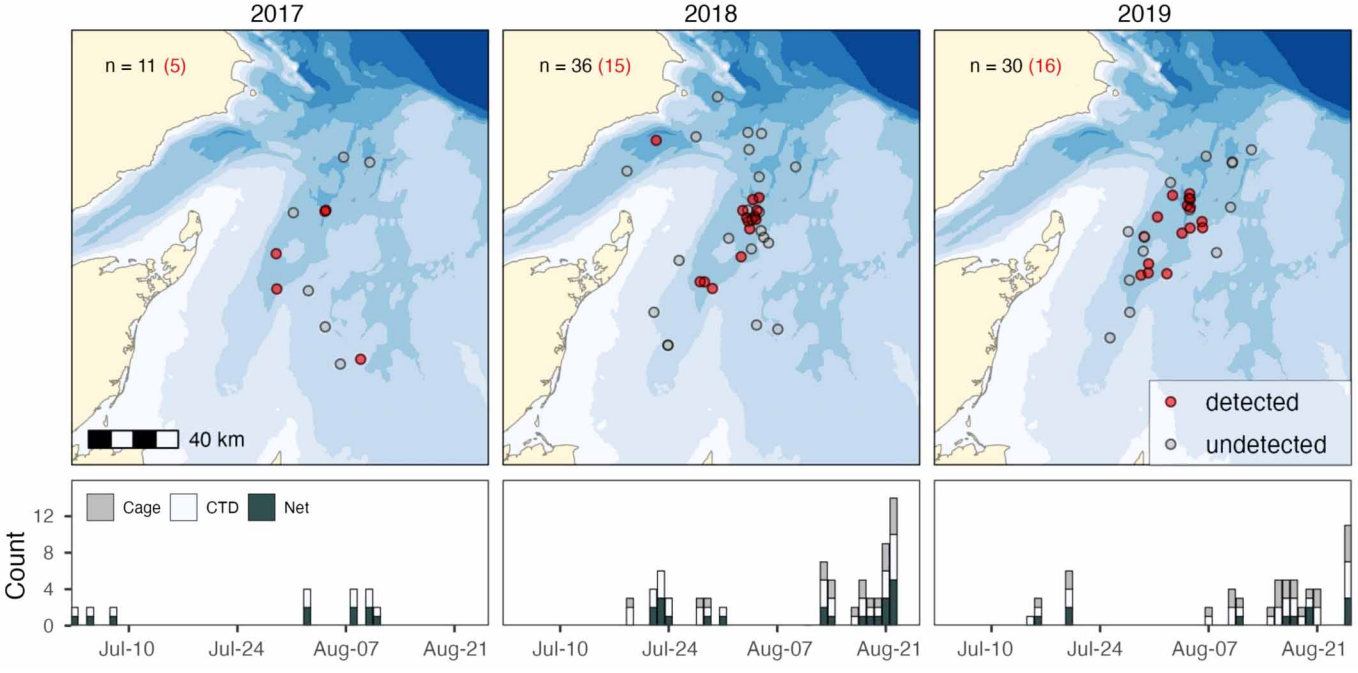

Fig. 2. Spatial and temporal distribution of sampling effort in 2017, 2018, and 2019. Dots on the maps: stations where whales were detected or undetected. Total number of stations each year (black text) as well as number with whales detected (red text in parentheses) are indicated in the upper left of each map panel. Lower panels show the count of cage (OPC/CTD), CTD, and net sampling events each day

3.2. Net samples

Depth-integrated zooplankton abundances derived from net sampling were highly variable. The samples tended to be numerically dominated by small copepods, such as small calanoid copepods (Table 1) which were the most abundant category of known right whale prey. Total abundance of small copepods was dominated by *Temora longicornus* and *Pseudocalanus* spp. (41 and 38% of small copepod abundance, respectively). *Centropages* spp., known right whale prey in Cape Cod Bay (e.g. Mayo & Marx 1990), comprised <5% of small copepod abundance. Median abundance of small calanoids at stations where whales were detected was 374 ind. m^{-3} (interquartile range [IQR]: 57–1079), which was 82% greater than the median abundance at stations where whales were not detected (206 ind. m^{-3}; IQR: 62–826), though, likely owing to high variability, there was no statistical evidence of higher abundance at stations where whales were detected (Table 1).

Median late-stage *Calanus finmarchicus* abundances were 78 ind. m^{-3} (IQR: 43–208) and 72 ind. m^{-3} (IQR: 36–124) at stations where whales were detected and undetected, respectively, which were statistically indistinguishable (Table 1). The abundances of *C. hyperboreus* were of a similar magnitude, but median abundance at stations where whales were present (68 ind. m^{-3}; IQR: 30–101) was significantly greater than median abundance at stations where whales were not detected (25 ind. m^{-3}; IQR: 9–46; Table 1). *C. glacialis* were relatively rare, with abundances typically less than 10 ind. m^{-3} (Fig. 3a). Median wet biomass (i.e. bulk wet weight of all collected zooplankton) was 0.47 g m^{-3} (IQR: 0.22–0.81) at stations where whales were detected, which was significantly higher than the biomass at stations where whales were not detected (0.22 g m^{-3}; IQR: 0.13–0.39; Fig. 3b, Table 1).

Small calanoid copepods comprised the greatest proportion of calanoid copepod abundance at all stations, followed by *C. finmarchicus*, *C. hyperboreus*, and *C. glacialis*. The proportions of each of these 4 groups

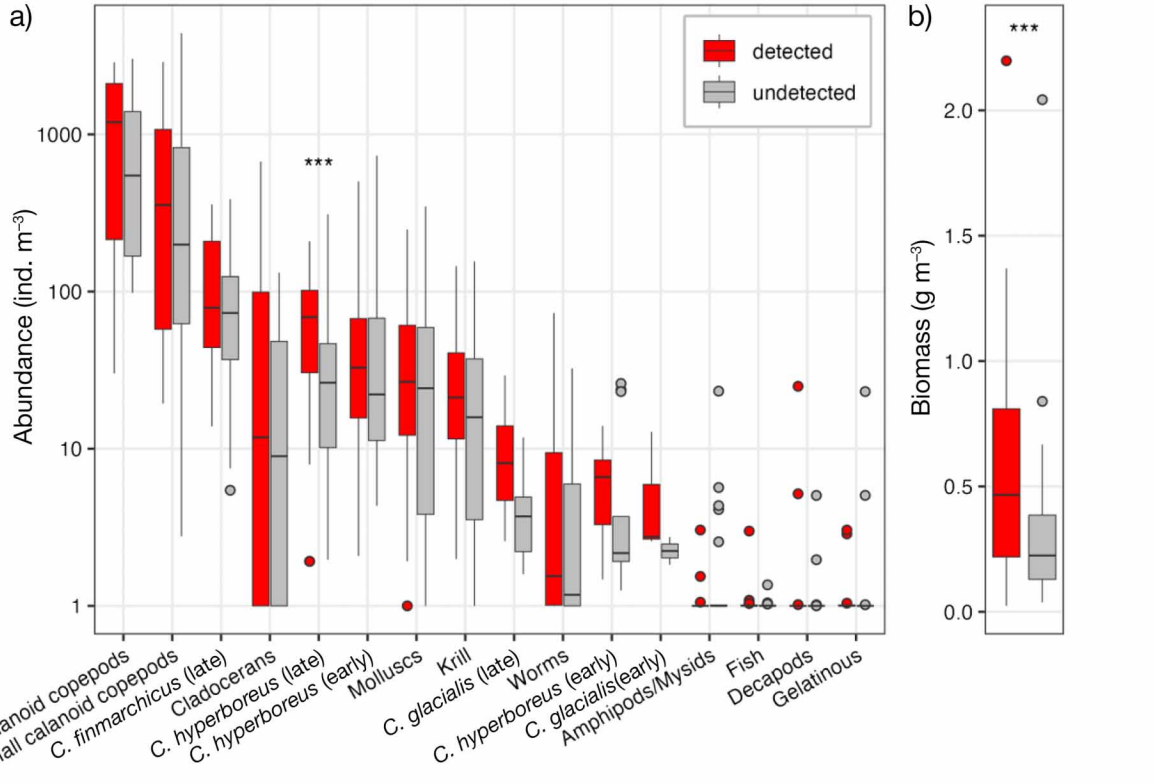

Fig. 3. (a) Box plots of the net-derived abundance of various zooplankton taxonomic groups at stations where right whales were detected (n = 20) or undetected (n = 24). Definitions of zooplankton groups provided in Table 1. A value of 1 was added to all abundances to facilitate plotting on a logarithmic scale. (b) Biomass (total wet weight) of all net contents (note that biomass was not available for one station where whales were detected, thus n = 19). ***: significant difference between stations where whales were detected versus undetected, evaluated using a Mann-Whitney *U*-test and $\alpha = 0.05$. Upper and lower quantiles define the top and bottom of each box median shown with a horizontal line. Upper and lower whiskers extend no further than 1.5 times the interquartile range to the largest and smallest values, respectively. Points outside that range are considered outliers and plotted individually

were indistinguishable between stations where whales were detected and undetected (Fig. 4a). Conversion from abundance to biomass using individual-specific dry weights revealed that *C. hyperboreus* typically comprised the majority of calanoid biomass (typically >50%). The relative biomass contribution of *C. hyperboreus* was slightly (~10%) greater and substantially less variable at stations where whales were detected versus undetected (Fig. 4b). Biomass contributions by small copepods and *C. glacialis* were low (≤5%). The typical contribution from *C finmarchicus* ranged from 20–40% at stations where whales were detected compared to 25–60% at stations where whales were not detected.

3.3. CTD and OPC

Averaged OPC profiles revealed peaks in particle abundance near the surface (5–15 m) and near the seafloor (85–100 m) in stations where whales were detected (Fig. 5a). Conversion to biomass and review of the size–frequency distribution of particles indicated that the near-surface peak was lower in biomass (Fig. 5b) and driven by small (<1.5 mm ESD) particles (Fig. 5c). In contrast, larger particles (>1.5 mm ESD) were much more abundant in the near-bottom peak (Fig. 5c), which contributed to the relatively large biomass below 80 m at stations where whales were detected (Fig. 5b). Because water depth at each station ranged from 60 to 100 m, the particle abundance and biomass below 60 m were only available from the deeper stations. To mitigate this issue, the same data were presented using height above the seafloor, rather than depth, to provide a common reference point for stations with different water depths. This revealed consistent maxima in both particle abundance and biomass within approximately 10–15 m of the seafloor at stations where whales were detected that were larger in magnitude and less variable than those derived from depth profiles (Fig. 6). The CTD data indicated a surface layer that extended to between 30 and 60 m depth, followed by the CIL below. There is evidence of slightly warmer, more saline water near the bottom in some profiles, but the bottom temperatures never exceeded the 1°C threshold used to distinguish the CIL from the deep layer that is typically present below 150 m in other regions of the GSL (Fig. 7; Fig. S1). The highest OPC-derived particle biomasses were found below 80 m depth and within 20 m of the sea floor (Figs. 5–7). The median bottom mixed layer thickness was 3.74 m (IQR: 1.75–7.75 m) at stations where whales were not detected and 7.00 m (IQR: 5.00–8.50 m) at stations where whales were detected. There was no difference between the minimum height above the sea floor achieved by the OPC profiles (9.0 ± 4.1 m; mean ± SD) and the net profiles (10.0 ± 3.6 m; 2 sample *t*-test, n = 26, $t = 0.91$, p = 0.37).

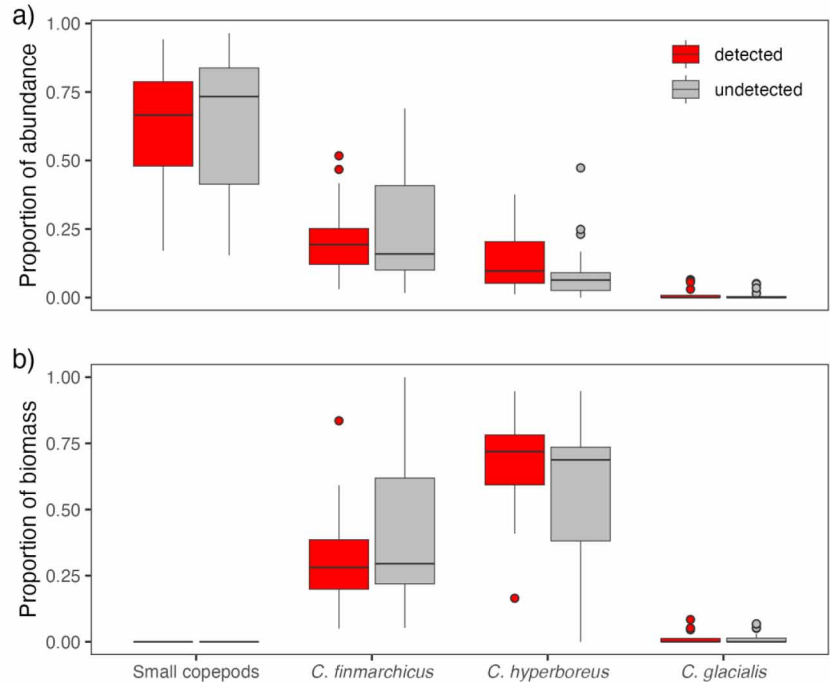

Fig. 4. Proportion of (a) abundance and (b) biomass of calanoid copepods collected from net samples from stations where right whales were detected (n = 20) and undetected (n = 24). Only late-stage (C4–C6) were considered for *Calanus* spp. Biomass (total dry weight) of *Calanus* spp. was estimated from abundance using species-, month-, and stage-specific individual dry weight conversions from Plourde et al. (2019). The small copepod group includes all calanoid copepods except *Calanus* spp. (see Table 1 for details). Upper and lower quantiles define the top and bottom of each box; median shown with a horizontal line. Upper and lower whiskers extend no further than 1.5 times the interquartile range to the largest and smallest values, respectively. Points outside that range are considered outliers and plotted individually

3.4. Logistic regression

Bottom depth and density at maximum sampled depth were significantly and positively associated with whale detection (Table 2) and highly correlated with one another (Fig. S2). Right whale detection was more likely with

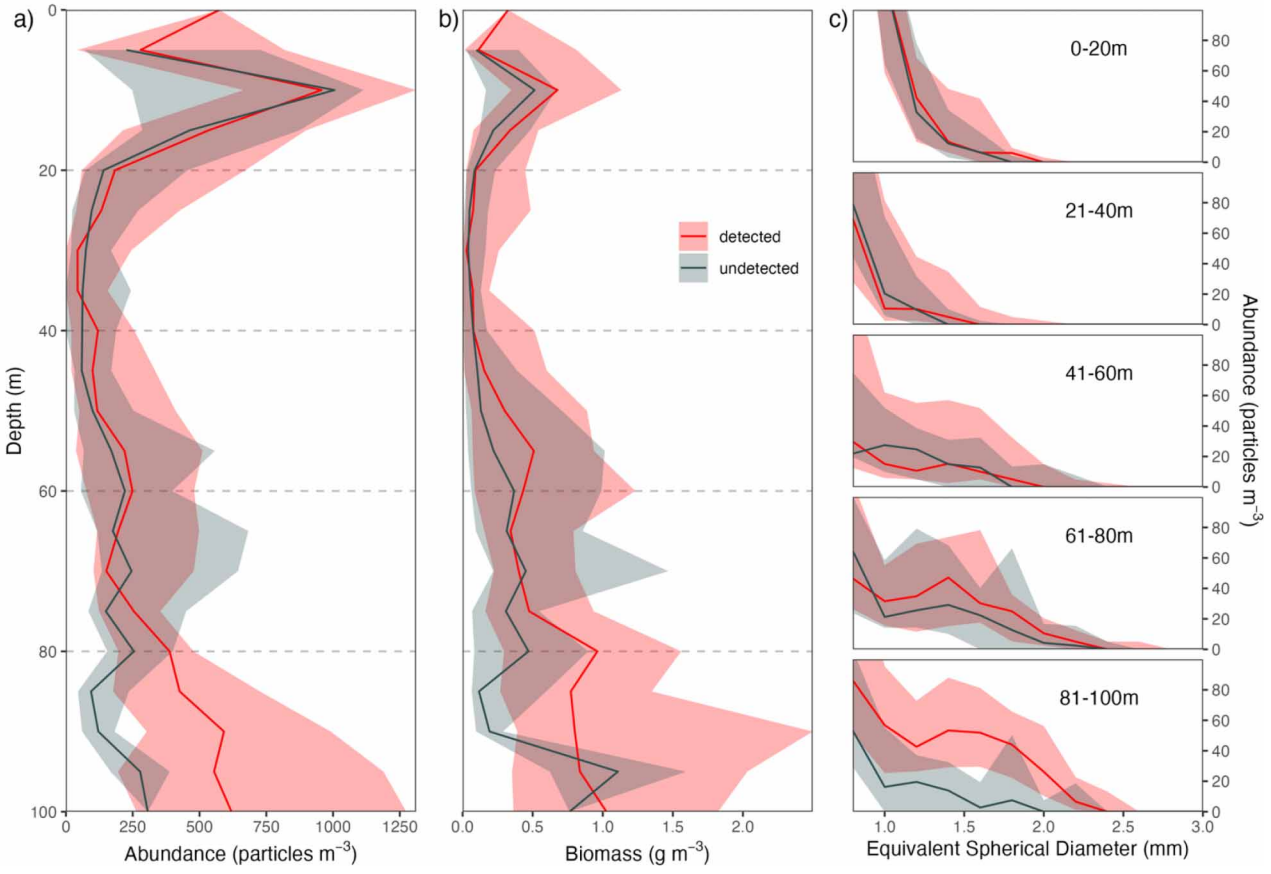

Fig. 5. Median (solid line) and interquartile range (shaded region) of optical plankton counter (OPC)-derived particle abundances from stations where right whales were detected (n = 23) or undetected (n = 19). (a) Vertical distribution of particles in the 0.8–5 mm equivalent spherical diameter (ESD) size range and 5 m depth bins. (b) Estimated biomass of particles in (a). (c) Size distribution of particles in 20 m depth strata and 0.2 mm ESD size bins. *x*-axis limits are restricted to 3 mm ESD because larger particles were rarely observed. Caution is warranted when interpreting data below 60 m (minimum station depth), as sample size is reduced. This issue is mitigated in Fig. 6, which expresses the same profiles in height above the seafloor

increasing thickness of the bottom mixed layer. It was also positively associated with the abundance of *C. hyperboreus*, the wet weight of the plankton collected in the net tow, and the maximum OPC biomass in the bottom 15 m of the cast (Table 2). The positive associations among whale detection and depth, bottom mixed layer thickness, maximum OPC biomass, and the maximum OPC biomass in the bottom 15 m were significant regardless of how whale detection was defined (see Text S1). In contrast, associations among whale detection and bottom density, surface mixed layer thickness, late-stage *C. hyperboreus* abundance, late-stage *Calanus* spp. abundance, and net biomass appeared to be more sensitive to the definition of whale detection, though this is confounded slightly by variation in sample size (Text S1). Notably, there was no association found between right whale detection and the abundance of *C. finmarchicus* derived from the net tows.

4. DISCUSSION

4.1. Right whale summertime foraging in the sGSL

Our analysis of the OPC data suggests that right whales in the sGSL in summer (July–August) are associated with a deep (80–100 m), abundant (>~500 ind. m^{-3}) layer of large (~1.5–3 mm ESD) mesozooplankton. The size of these mesozooplankton is consistent with late-stage *Calanus*, though it is not possible to confidently disentangle the relative contributions of *C. finmarchicus* and *C. hyperboreus* in this deep layer from our OPC data owing to their overlapping size distributions (Herman 1992, Davies et al. 2014). The size–frequency distribution of particles in the deep layer (Fig. 6c) had the characteristic 'bump' that previous studies had associated with the presence of stage C5 *C. finmarchicus* (Herman 1992, Edvardsen 2002, Baumgartner 2003), and the logistic regression provided

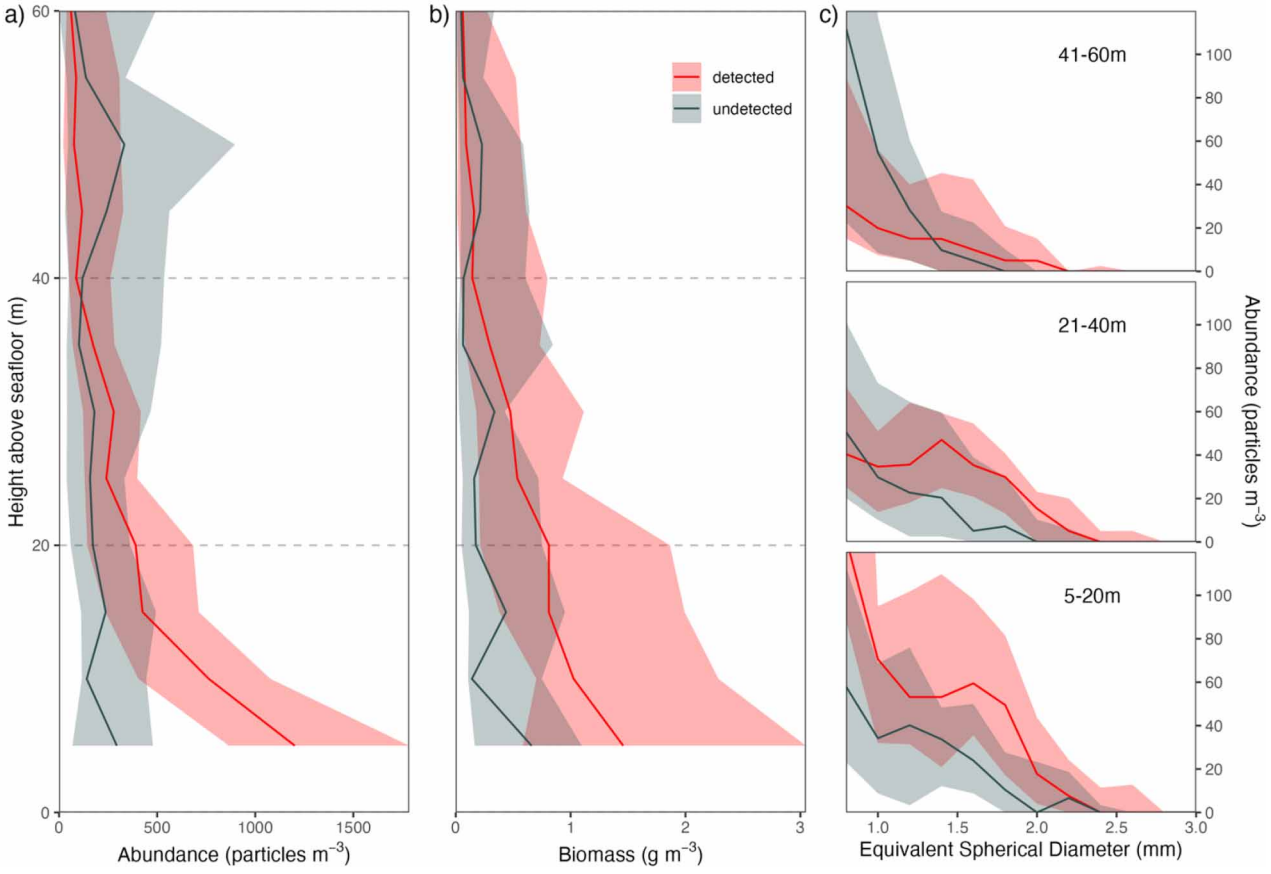

Fig. 6. Median (solid line) and interquartile range (shaded region) of optical plankton counter (OPC)-derived particle abundances from stations where right whales were detected (n = 23) or undetected (n = 19). (a) Distribution of particles in the 0.8–5 mm equivalent spherical diameter (ESD) size range and 5 m depth bins in height above the seafloor, rather than in depth from the surface (see Fig. 5). Using height above the seafloor provides a common reference point for stations with different water depths. Height is truncated above 60 m to remove artifacts caused by stations with different water depths, and below 5 m as we were typically unable to sample close to the bottom. (b) Estimated biomass of particles in (a). (c) Size distribution of particles in 20 m height strata and 0.2 mm ESD size bins. *x*-axis limits are restricted to 3 mm ESD because larger particles were rarely observed. Note the characteristic 'bump' in particle size between 1.5 and 2.0 mm in the 5–20 m stratum of (c) for stations where whales were detected (red) that previous studies have associated with the presence of C5 *Calanus finmarchicus* (Herman 1992, Edvardsen 2002, Baumgartner 2003)

strong evidence of an association between right whale detection and particle abundance in the size range of late-stage *Calanus* (opc_deep_max, p = 0.019; Table 2), but our analysis of the net data provided modest evidence of a relationship between whale detection and the net-derived biomass of *C. hyperboreus* (net_hyperboreus, p = 0.050; Table 2, Fig. 4b), not *C. finmarchicus* (net_finmarchicus, p = 0.246; Table 2, Fig. 4b). We therefore conclude that right whales are feeding on a community of large-bodied copepods that is most likely comprised of both *C. finmarchicus* and *C. hyperboreus*.

These observations of right whales apparently targeting late-stage *Calanus* spp. confirms what previous studies have assumed based on knowledge of right whale foraging ecology, regional zooplankton sampling and/or simulations (Brennan et al. 2019, 2021, Plourde et al. 2019, Sorochan et al. 2019, Gavrilchuk et al. 2021), or fine-scale sampling in right whale high-use areas (Sorochan et al. 2023). The mixed assemblage of *C. hyperboreus* and *C. finmarchicus* clearly distinguishes the sGSL from previously studied right whale feeding habitats in the lower Bay of Fundy (Murison & Gaskin 1989, Baumgartner et al. 2003b, Michaud & Taggart 2011) and Great South Channel (Beardsley et al. 1996) in which *C. finmarchicus* C5 was the focal prey, as well as Cape Cod Bay, where whales tend to feed on smaller calanoid copepods in late winter (Mayo & Marx 1990). The Roseway Basin habitat on the Scotian Shelf may also contain a mixed assemblage of *C. hyperboreus* and *C. finmarchicus*, but the proportion of *C. hyperboreus* is highly variable,

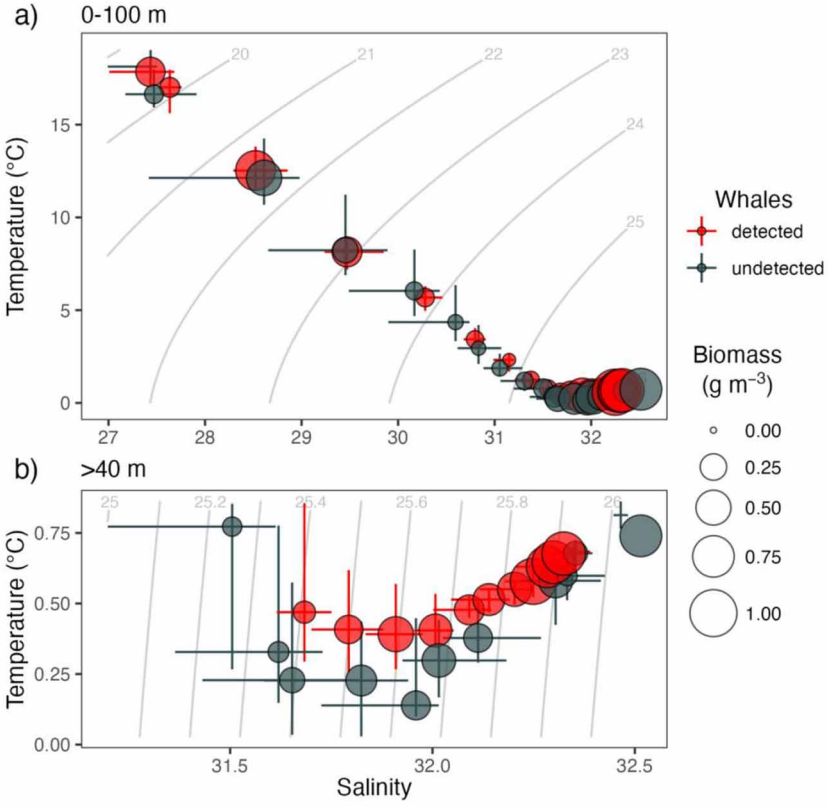

Fig. 7. Optical plankton counter (OPC)-derived particle biomass in stations where right whales were detected (n = 23) or undetected (n = 19) in temperature–salinity space. Vertical and horizontal bars represent interquartile range of temperature and salinity values over 5 m depth bins, respectively, and intersect at the median. Sizes of the filled circles correspond to the median particle biomass in the same 5 m depth bins (from Fig. 5). Grey contour lines indicate water density (kg m^{-3} − 1000) isopycnals. (a) Depths from 0–100 m; (b) detailed view of depths >40 m

as these copepods are expatriots advected from northern waters rather than local production (Davies et al. 2014, 2015). Though the opportunistic nature of our observations prevents more rigorous statistical analyses, our results provide insights into the biophysical mechanisms responsible for aggregating right whale prey in this habitat and spark numerous questions to be explored in more detail in the future.

There was little evidence to support the possibility that right whales were targeting other, non-copepod zooplankton prey. The net data did not reveal any obvious indications that alternative taxa were present in sufficient abundance to warrant consideration as a substantial, consistent prey resource. However, our zooplankton analysis was restricted to enumerating individual taxa and measuring bulk (full sample) biomass, and as a result we lack information necessary to quantify the potential biomass or energetic contribution of each taxa. At 30% (6 out of 20) stations where whales were detected, the abundances of the small calanoid copepods exceeding the feeding threshold suggested for Cape Cod Bay (1000 ind. m^{-3}; Mayo & Marx 1990). It is possible that right whales supplement their foraging on large *Calanus* spp. with consumption of these smaller copepods; however, it should be noted that these smaller species also have much smaller energy densities when compared to late-stage *Calanus* spp. Another possibility is that right whales are preying upon taxa that are large and mobile enough to evade capture by our sampling equipment. Perhaps the most likely candidate would be euphausiids, on which right whales in other regions are known to feed (Collett 1909, Hamner et al. 1988) and are abundant in the sGSL (e.g. McQuinn et al. 2015). Further study, such as analysis of fecal content, is required to explore these and other potential alternative foraging strategies in greater detail.

4.2. Biophysical mechanisms affecting sGSL habitat quality

The difference in size between *C. hyperboreus* and *C. finmarchicus* has important implications for right whale foraging. Though their energy densities (i.e. energy per unit body mass) are similar (Davies et al. 2012), a single adult *C. hyperboreus* is up to 6 times larger (by mass) than an adult *C. finmarchicus*. This energetic distinction between *C. finmarchicus* and *C. hyperboreus* is important to consider when evaluating or comparing the potential suitability of right whale foraging habitats. Using abundance to define feeding thresholds is appropriate and common practice in habitats strongly dominated by *C. finmarchicus*, but in habitats like the sGSL with a more mixed assemblage of *Calanus* spp. it is preferable to conduct comparisons using biomass, or, ideally, energy content. To illustrate this concept, we provide a simple comparison between depth-integrated net samples collected near right whales in the sGSL (this study) and in the lower Bay of Fundy (BOF) in 1999–2001 (Baumgartner et al. 2003a; Fig. 8). C*alanus* spp. abundances in the BOF were nearly an order of magnitude greater than those in the sGSL (on the order of 1000 in BOF vs. the order of 100 ind. m^{-3} in sGSL) and driven almost entirely by

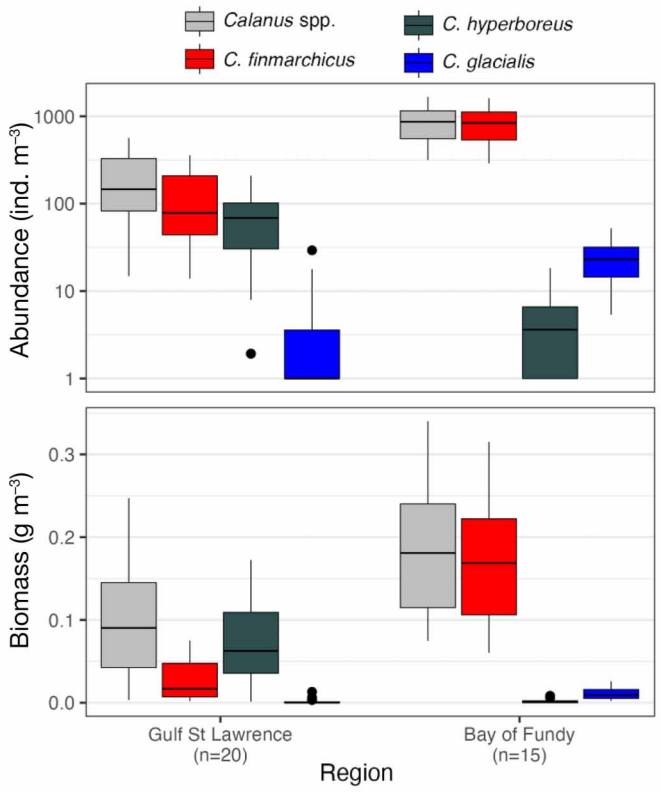

Fig. 8. Abundance and estimated biomass of late-stage (C4–C6) *Calanus finmarchicus*, *C. hyperboreus*, *C. glacialis* and sum total of all 3 species *Calanus* species collected using depth-integrated net tows near right whales in the southern Gulf of St. Lawrence in 2017–2019 (this study; n = 20) and the lower Bay of Fundy (n = 15) in 1999–2001 (Baumgartner et al. 2003b). Biomass (total dry weight) of *Calanus* spp. in the Gulf of St Lawrence was estimated from abundance using species-, month-, and stage-specific individual dry weight conversions from Plourde et al. (2019), as in Fig. 4. Biomass of *Calanus* spp. in the lower Bay of Fundy was estimated from abundance using species- and stage-specific individual dry weight conversions from Head & Harris (2004). Note that abundance is shown on a logarithmic scale, and a value of 1 was added to all abundances to facilitate logarithmic plotting. Upper and lower quantiles define the top and bottom of each box; median is shown with a horizontal line. Upper and lower whiskers extend no further than 1.5 times the interquartile range to the largest and smallest values, respectively. Points outside that range are considered outliers and plotted individually

C. finmarchicus while the sGSL abundance is almost equally split between *C. finmarchicus* and *C. hyperboreus*. Upon converting to biomass, the low overall abundance in the sGSL is heavily compensated by the larger size of *C. hyperboreus* such that the total biomass estimates from each site are of the same order of magnitude (ranging from 0.5–2.5 g m^{-3}).

Differences in the life histories of *C. finmarchicus* and *C. hyperboreus* also influence the composition and quality of prey available to right whales throughout the season. *C. finmarchicus* is an income breeder, meaning it uses concurrent food intake to produce eggs during its feeding season and is therefore capable of completing multiple reproductive cycles within a single year given sufficient resources (e.g. Plourde & Runge 1993). In contrast, *C. hyperboreus* is a capital breeder, using lipid reserves accumulated the previous year to produce eggs during winter and only undergoing a single reproductive cycle each year (e.g. Plourde et al. 2003; see Sainmont et al. 2014 for a comparison of capital vs. income breeding). One consequence of this distinction is that the production cycle of *C. finmarchicus* is more strongly coupled to seasonal primary productivity. This distinction is reflected in the stage composition of each species we observed during summer, where 55% of *C. finmarchicus* were stage C4–C6 compared to 91% of *C. hyperboreus*, suggesting many *C. finmarchicus* are actively reproducing while *C. hyperboreus* have already reproduced and entered diapause (Fig. S3). This is consistent with previous work documenting *C. hyperboreus* entering diapause in the sGSL in the spring, while *C. finmarchicus* may continue to reproduce throughout the summer (e.g. Sorochan et al. 2021b), resulting in a higher proportion of late-stage *C. finmarchicus* than *C. hyperboreus* in the late summer and fall. This suggests that the community composition (i.e. the relative proportions of *C. finmarchicus* and *C. hyperboreus*) in the prey patches upon which right whales feed changes over the period of time that right whales are present in the sGSL and that the relative importance of *C. finmarchicus* for right whale foraging likely increases later in the year.

Brennan et al. (2019) concluded that the accumulation of *Calanus* spp. in the sGSL occurs primarily through the transport of active stages via the Gaspé Current and their local transition into diapause. In all study years (2017–2019), the environmental conditions, namely high runoff from the St. Lawrence River, favored the coastal attachment of the Gaspé Current and subsequent transport and retention of *Calanus* to and within the sGSL (Galbraith et al. 2020, Brennan et al. 2021). This suggests that the dense layer of *Calanus* near the bottom that we observed is formed via Gaspé Current transport and local vertical migration, rather than by an intrusion of warm, saline water from the Laurentian Channel. A simulation study by Le Corre et al. (2023) suggested that 52–66% of the biomass of *C. hyperboreus* in the Shediac Valley originated from a region comprising the St Laurence Estuary and area west of Anticosti Island. The possible association between OPC-derived biomass and the bottom mixed layer thickness is therefore likely not in-

dicative of *Calanus* being advected in deep water mass intrusions from the nearby slope, as has been documented in Roseway Basin (Davies et al. 2014), but more likely occurs as the result of *Calanus* entering diapause and forming aggregations near the sea floor.

The bottom mixed layer depth appears to play an important role in right whale foraging in several right whale feeding habitats, including the sGSL, but through different mechanisms. A positive association between the thickness of the bottom mixed layer and whale detection, as we have documented in the sGSL, has also been observed in the lower Bay of Fundy and Roseway Basin. Baumgartner & Mate (2003) observed that the thin, dense layers of *C. finmarchicus* upon which right whales fed occurred just above the top of the bottom mixed layer, and Baumgartner et al. (2003b) observed a positive association between bottom mixed layer thickness and right whale occurrence, just as was observed in the present study. Baumgartner et al. (2003b) proposed that a thick bottom mixed layer made the associated prey layer comparatively more available to air-breathing right whales (i.e. closer to the sea surface) than a prey layer over a thin bottom mixed layer in waters with the same bottom depth. In Roseway Basin, there is evidence that a deeper 1026 kg m^{-3} isopycnal, in combination with tidal currents and the basin margin, functions to concentrate *C. finmarchicus* near the seafloor (Davies et al. 2014). It would seem that the dynamics in the sGSL are similar to those in the lower BOF, where a thick bottom mixed layer makes *Calanus* more available to right whales. If this were the case, we would expect occasional profiles where we vertically sample through this layer. This was not readily apparent in our dataset, perhaps owing to our sampling too far from feeding whales (i.e. farther than the extent of a hyperdense patch of *Calanus* spp.) or near-bottom sampling limitations described in more detail below, but has been observed by others collecting similar data in the region (Sorochan et al. 2023). Further, given that the BOF is deeper than the sGSL (~200 vs. ~100 m) and can have a much thicker bottom mixed layer (30–70 vs. 2–10 m), the bottom mixed layer dynamics may have a greater impact on prey availability for right whales in the BOF versus the sGSL.

4.3. Conclusions, caveats, and recommendations for future sampling

Our study was only possible because we were able to conduct oceanographic and prey field sampling on an opportunistic, non-interference basis with ongoing visual surveys. This resulted in a non-systematic, non-random sampling design that was biased towards times and places with known whale presence. This renders us unable to conduct robust temporal or spatial comparisons and warrants precautionary treatment of the p-values of the logistic regression analysis. We would consider it inappropriate to apply these statistical relationships in a predictive capacity, especially in other regions. Although the variability in our survey effort and the cryptic behavior of right whales made it challenging to confirm whale absence, we developed our definitions of whale detection carefully such that sampling at stations where whales were detected occurred in close proximity to whales, while sampling at stations where whales were not detected likely did not.

Our relatively small sample size and the opportunistic sampling strategy we employed prevented us from making more detailed insights into temporal and spatial variation in zooplankton dynamics, such as diel vertical migration or seasonal shifts in community composition. The use of a platform of opportunity (i.e. smaller motor vessel or larger fishing vessel) also posed challenges for oceanographic data collection, chief among which was our inability to consistently sample in close proximity (within ~10 m) to the seafloor without risking damage to our equipment. We sought to mitigate this limitation by only including profiles that traversed at least 85% of the water column, but in most cases the lower 5–10% of the water column (typically ~2–10 m from the sea floor) remained unsampled. As a consequence, we are likely systematically underestimating the abundance of the deep zooplankton layer that right whales are likely feeding upon. Right whales regularly dive to the sea floor across habitats (Baumgartner et al. 2017) and in some habitats are commonly observed with mud-covered heads from making contact with the sea floor (Hamilton & Kraus 2019). This undersampling could be mitigated in future studies by using nets designed to interact with the bottom (e.g. tucker trawls), employing active acoustic sensors (e.g. echosounders), and/or improving the real-time depth reporting of the profiling systems (e.g. monitor instrument depth using conductive cable).

The zooplankton patches on which right whales forage can be extremely localized in horizontal (<500 m) and vertical (1–2 m) space (e.g. Baumgartner et al. 2003a, Sorochan et al. 2021b, 2023). Though we attempted to only analyze samples collected in close proximity to whales, it is possible that, due to limitations in our survey design, we were unable to consistently sample within the zooplankton patch on which

right whales were feeding. As a result, we may be underestimating zooplankton abundance that right whales are actively targeting and feeding upon. This may at least partially explain why the observed differences in zooplankton abundances between stations where whales were detected versus undetected were relatively small. Another possible explanation is that some of the whales we sampled near were not actively foraging. These issues could be mitigated by designing future studies capable of identifying foraging behavior (perhaps using animal-borne tags) and conducting high-resolution prey sampling along the path of the foraging whale (e.g. Baumgartner et al. 2017).

Another important consideration when interpreting zooplankton data from a right whale habitat is the distinction between regional average, or 'background', abundance, such as those determined via systematic zooplankton sampling programs, versus abundance from samples collected in proximity to right whales. The thin, dense patches of *Calanus* spp. right whales forage upon may be more likely to form when baseline zooplankton levels are high (e.g. Pendleton et al. 2009), but this baseline is not necessarily representative of the prey available to right whales (Baumgartner et al. 2003b). While regional abundance estimates, such as those developed by Sorochan et al. (2019), are extremely valuable tools to understand long-term (e.g. interannual, decadal) variability in habitat quality, they would substantially underestimate absolute energy available to right whales because whales are better at finding high density mesozooplankton patches than random net sampling of a patchy prey field. For example, the median biomass of *Calanus* spp. in net samples we collected in the sGSL in the presence of right whales (~14 300 mg m^{-2}) was an order of magnitude larger than the June–July average from annual sampling (years 1999–2016) at the Shediac valley station (~1000 mg m^{-2}; Sorochan et al. 2019). The use of average prey densities from regional sampling and/or model predictions could explain why bioenergetic models developed by Gavrilchuk et al. (2021) predicted that the available biomass in the sGSL may be insufficient to support the energetic costs of reproduction despite empirical evidence of greater reproductive success in the portion of the population that regularly visit the sGSL (Bishop et al. 2022).

Our results complement numerous recent and ongoing efforts to better characterize the habitat and feeding ecology of right whales in the sGSL. We provide evidence that right whales are targeting a mixed assemblage of late-stage *C. finmarchicus* and *C. hyperboreus* concentrated near the bottom primarily within the Shediac Valley. Our *Calanus* biomass estimates are considerably higher than those derived from systematic regional sampling, which must be considered when assessing habitat suitability and the ability of right whales to meet their energetic needs. Future efforts ought to expand the temporal and spatial extent of sampling, ideally using a systematic framework that is more conducive to the development of rigorous statistical associations between oceanographic conditions, zooplankton dynamics, and right whale occurrence. These efforts should employ modified sampling methods that facilitate the enumeration of the near-bottom zooplankton community and perhaps include a biologging (i.e. time/depth recorders) component to characterize right whale movement within the prey field. Such studies may allow for the development of short-term (weeks to months) predictive models of right whale occurrence and distribution within the sGSL that could be employed to better inform management measures and improve conservation outcomes.

Acknowledgements. We are indebted to Martin Noël, Guy Lanteigne, Jean-Denis Noël, the late Joe Howlett, and David Anthony for their assistance, good humor, and expert operation of the research vessels used in this work. We are grateful for the tireless efforts and patience of those who helped conduct this fieldwork, including Pam Emery, Megan McOsker, Pete Duley, Monica Zani, Kelsey Howe, Marianna Hagbloom, and Marcia Pearson. We thank Angelia Vanderlaan, Valentina Ceballos, Gina Lonati and Kevin Sorochan for helpful discussions. We also thank Sarah Haney for generously providing the M/V 'Shelagh' for surveys in 2017. Walter Judge, Daniel Morrison, Richard Cheel and Mark Merrimen provided invaluable technical support. Support for this study was provided by the Department of Fisheries and Oceans, Natural Sciences and Engineering Research Council of Canada, the Habitat Stewardship Program, the Marine Environmental Prediction and Response Network, World Wildlife Fund, and the Canadian Whale Institute. Additional support for visual surveys was provided to the New England Aquarium by Irving Oil and the Island Foundation. The present work was part of H.D.J.'s PhD thesis at Dalhousie University. Support for H.D.J. was provided by the Killam Foundation, Vanier Canada Graduate Scholarship program, Dalhousie University, the Nova Scotia Graduate Scholarship program, and the Canada Graduate Scholarships — Michael Smith Foreign Study Supplements program. The work was conducted under the following SARA permits issues to the New England Aquarium under section 73: DFO-GLF-2017-01 and DFO-GLF-2017-01 amended on 2018-07-11. We dedicate this work to the memory of our beloved colleague, friend, and captain Joe Howlett.

LITERATURE CITED

Baumgartner MF (2003) Comparisons of *Calanus finmarchicus* fifth copepodite abundance estimates from nets and an optical plankton counter. J Plankton Res 25:855–868

Baumgartner MF, Mate BR (2003) Summertime foraging ecology of North Atlantic right whales. Mar Ecol Prog Ser 264:123–135

Baumgartner MF, Tarrant AM (2017) The physiology and ecology of diapause in marine copepods. Annu Rev Mar Sci 9:387–411

Baumgartner MF, Cole TVN, Campbell RG, Teegarden GJ, Durbin EG (2003a) Associations between North Atlantic right whales and their prey, *Calanus finmarchicus*, over diel and tidal time scales. Mar Ecol Prog Ser 264: 155–166

Baumgartner MF, Cole TVN, Clapham PJ, Mate BR (2003b) North Atlantic right whale habitat in the lower Bay of Fundy and on the SW Scotian Shelf during 1999–2001. Mar Ecol Prog Ser 264:137–154

Baumgartner MF, Mayo CA, Kenney RD (2007) Enormous carnivores, microscopic food, and a restaurant that's hard to find. In: Kraus SD, Rolland RM (eds) The urban whale: North Atlantic right whales at the crossroads. Harvard University Press, Cambridge, MA, p 138–171

Baumgartner MF, Wenzel FW, Lysiak NSJ, Patrician MR (2017) North Atlantic right whale foraging ecology and its role in human-caused mortality. Mar Ecol Prog Ser 581:165–181

Beardsley RC, Epstein AW, Chen C, Wishner KF, Macaulay MC, Kenney RD (1996) Spatial variability in zooplankton abundance near feeding right whales in the Great South Channel. Deep Sea Res II 43:1601–1625

Bishop AL, Crowe LM, Hamilton PK, Meyer-Gutbrod EL (2022) Maternal lineage and habitat use patterns explain variation in the fecundity of a critically endangered baleen whale. Front Mar Sci 9:880910

Bourque L, Wimmer T, Lair S, Jones M, Daoust PY (2020) Incident report: North Atlantic right whale mortality event in Eastern Canada 2019. Collaborative Report Produced by: Canadian Wildlife Health Cooperative and Marine Animal Response Society. https://www.cwhc-rcsf.ca/docs/2019%20NARW%20incident%20report_June%202020.pdf

Brennan CE, Maps F, Gentleman WC, Plourde S and others (2019) How transport shapes copepod distributions in relation to whale feeding habitat: demonstration of a new modelling framework. Prog Oceanogr 171:1–21

Brennan CE, Maps F, Gentleman WC, Lavoie D, Chassé J, Plourde S, Johnson CL (2021) Ocean circulation changes drive shifts in *Calanus* abundance in North Atlantic right whale foraging habitat: a model comparison of cool and warm year scenarios. Prog Oceanogr 197:102629

Brown MW, Kraus SD, Slay CK, Garrison LP (2007) Surveying for discovery, science and management. In: Kraus SD, Rolland RM (eds) The urban whale: North Atlantic right whale at the crossroads. Harvard University Press, Cambridge, MA, p 105–137

Brown MW, Fenton DG, Smedbol RK, Merrimen C, Robichaud-Leblanc K, Conway J (2009) Recovery strategy for the North Atlantic right whale (*Eubalaena glacialis*) in Atlantic Canadian waters. Fisheries and Oceans Canada, Ottawa

Ceballos V, Taggart C, Johnson H (2023) Comparison of visual and acoustic surveys for the detection and dynamic management of North Atlantic right whales (*Eubalaena glacialis*) in Canada. Conserv Sci Pract 5:e12866

Chamberlain SA, Szöcs E (2013) Taxize: taxonomic search and retrieval in R. F1000 Res

Chang W, Cheng J, Allaire JJ, Xie Y, McPherson J (2020) shiny: web application framework for R. https://shiny.posit.co/

Collett PR (1909) A few notes on the whale *Balæna glacialis* and its capture in recent years in the North Atlantic by Norwegian whalers. Proc Zool Soc Lond 79:91–103

Crowe LM, Brown MW, Corkeron PJ, Hamilton PK and others (2021) In plane sight: a mark-recapture analysis of North Atlantic right whales in the Gulf of St. Lawrence. Endang Species Res 46:227–251

Daoust P, Couture E, Wimmer T, Bourque L (2017) Incident report: North Atlantic right whale mortality event in the Gulf of St. Lawrence, 2017. Collaborative Report Produced by: Canadian Wildlife Health Cooperative and Marine Animal Response Society. https://www.cwhc-rcsf.ca/docs/technical_reports/NARW_Incident_Report-%2020180405%20MD.pdf

Davies KTA, Brillant SW (2019) Mass human-caused mortality spurs federal action to protect endangered North Atlantic right whales in Canada. Mar Policy 104:157–162

Davies KTA, Ryan A, Taggart CT (2012) Measured and inferred gross energy content in diapausing *Calanus* spp. in a Scotian shelf basin. J Plankton Res 34:614–625

Davies KTA, Ross T, Taggart CT (2013) Tidal and subtidal currents affect deep aggregations of right whale prey, *Calanus* spp., along a shelf-basin margin. Mar Ecol Prog Ser 479:263–282

Davies KTA, Taggart CT, Smedbol RK (2014) Water mass structure defines the diapausing copepod distribution in a right whale habitat on the Scotian Shelf. Mar Ecol Prog Ser 497:69–85

Davies KTA, Taggart CT, Smedbol RK (2015) Interannual variation in diapausing copepods and associated water masses in a continental shelf basin, and implications for copepod buoyancy. J Mar Syst 151:35–46

Davies KTA, Brown MW, Hamilton PK, Knowlton AR, Taggart CT, Vanderlaan ASM (2019) Variation in North Atlantic right whale *Eubalaena glacialis* occurrence in the Bay of Fundy, Canada, over three decades. Endang Species Res 39:159–171

Davis GE, Baumgartner MF, Bonnell JM, Bell J and others (2017) Long-term passive acoustic recordings track the changing distribution of North Atlantic right whales (*Eubalaena glacialis*) from 2004 to 2014. Sci Rep 7:13460

DFO (2017) Critical habitat of the North Atlantic right whale (*Eubalaena glacialis*) order (SOR/2017-262). https://laws-lois.justice.gc.ca/eng/regulations/SOR-2017-262/page-1.html (accessed 31 Jan 2023)

Dunnington D (2021) ggspatial: spatial data framework for ggplot2. https://paleolimbot.github.io/ggspatial/

Durette-Morin D, Evers C, Johnson HD, Kowarski K and others (2022) The distribution of North Atlantic right whales in Canadian waters from 2015–2017 revealed by passive acoustic monitoring. Front Mar Sci 9:976044

Edvardsen A (2002) Determining zooplankton ESD signatures using an in situ OPC in the laboratory. In: Zhou M, Tande K (eds) Optical plankton counter workshop. GLOBEC Report 17. GLOBEC International Project Office, Plymouth, p 16–21

Fleminger A, Clutter RI (1965) Avoidance of towed nets by zooplankton. Limnol Oceanogr 10:96–104

Fortune SME, Ferguson SH, Trites AW, Hudson JM, Baumgartner MF (2020) Bowhead whales use two foraging strategies in response to fine-scale differences in zooplankton vertical distribution. Sci Rep 10:20249

Galbraith PS, Chassé J, Shaw JL, Dumas J, Caverhill C,

Lefaivre D, Lafleur C (2020) Physical oceanographic conditions in the Gulf of St. Lawrence during 2019. DFO Can Sci Advis Sec Res Doc 2020/030

Gavrilchuk K, Lesage V, Fortune SME, Trites AW, Plourde S (2021) Foraging habitat of North Atlantic right whales has declined in the Gulf of St. Lawrence, Canada, and may be insufficient for successful reproduction. Endang Species Res 44:113–136

Hamilton PK, Kraus SD (2019) Frequent encounters with the seafloor increase right whales' risk of entanglement in fishing groundlines. Endang Species Res 39:235–246

Hamilton PK, Knowlton AR, Marx MK (2007) Right whales tell their own stories: the photo-identification catalog. In: The urban whale: North Atlantic right whales at the crossroads. Harvard University Press, Cambridge, MA, p 75–104

Hamner WM, Stone GS, Obst BS (1988) Behavior of southern right whales, *Eubalaena australis*, feeding on the Antarctic krill, *Euphausia superba.* Fish Bull 86:143–150

Head EJH, Harris LR (2004) Estimating zooplankton biomass from dry weights of groups of individual organisms. Canadian Science Advisory Secretariat Research Document 2004/045

Herman AW (1992) Design and calibration of a new optical plankton counter capable of sizing small zooplankton. Deep-Sea Res 39:395–415

Horton T, Kroh A, Ahyong S, Bailly N and others (2021) World register of marine species (WoRMS). https://www.marinespecies.org/

Johnson HD (2021) opcr: process and plot data from an optical plankton counter, v1.0.0. Zenodo.

Johnson H, Morrison D, Taggart C (2021) WhaleMap: a tool to collate and display whale survey results in near real-time. J Open Source Softw 6:3094

Kelley D, Richards C (2025) oce: analysis of oceanographic data. R package version 1.8-4. https://dankelley.github.io/oce/

Klymentieva H (2022) Prey field characteristics of North Atlantic right whales in the southern Gulf of St. Lawrence. BSc (Hon) thesis. University of New Brunswick, Saint John

Knowlton AR, Hamilton PK, Marx MK, Pettis HM, Kraus SD (2012) Monitoring North Atlantic right whale *Eubalaena glacialis* entanglement rates: a 30 yr retrospective. Mar Ecol Prog Ser 466:293–302

Knowlton AR, Clark JS, Hamilton PK, Kraus SD, Pettis HM, Rolland RM, Schick RS (2022) Fishing gear entanglement threatens recovery of critically endangered North Atlantic right whales. Conserv Sci Pract 4:e12736

Kraus SD (1990) Rates and potential causes of mortality in North Atlantic right whales (*Eubalaena glacialis*). Mar Mamm Sci 6:278–291

Kraus SD, Moore KE, Price CA, Crone MJ and others (1986) The use of photographs to identify individual North Atlantic right whales (*Eubalaena glacialis*). Rep Int Whaling Comm 10:145–151

Kraus SD, Brown MW, Caswell H, Clark CW and others (2005) North Atlantic right whales in crisis. Science 309: 561–562

Le Corre N, Brennan CE, Chassé J, Johnson CL and others (2023) A biophysical model of *Calanus hyperboreus* in the Gulf of St. Lawrence: interannual variability in phenology and circulation drive the timing and location of right whale foraging habitat in spring and early summer. Prog Oceanogr 219:103152

Leiter SM, Stone KM, Thompson JL, Accardo CM and others (2017) North Atlantic right whale *Eubalaena glacialis* occurrence in offshore wind energy areas near Massachusetts and Rhode Island, USA. Endang Species Res 34: 45–59

Lu Y, Thompson KR, Wright DG (2001) Tidal currents and mixing in the Gulf of St. Lawrence: an application of the incremental approach to data assimilation. Can J Fish Aquat Sci 58:723–735

Mayo CA, Marx MK (1990) Surface foraging behaviour of the North Atlantic right whale, *Eubalaena glacialis*, and associated zooplankton characteristics. Can J Zool 68: 2214–2220

Mayo CA, Letcher BH, Scott S (2001) Zooplankton filtering efficiency of the baleen of a North Atlantic right whale, *Eubalaena glacialis*. JCRM:225–229

Mayo CA, Ganley L, Hudak CA, Brault S, Marx MK, Burke E, Brown MW (2018) Distribution, demography, and behavior of North Atlantic right whales (*Eubalaena glacialis*) in Cape Cod Bay, Massachusetts, 1998–2013. Mar Mamm Sci 34:979–996

McQuinn IH, Plourde S, St. Pierre JF, Dion M (2015) Spatial and temporal variations in the abundance, distribution, and aggregation of krill (*Thysanoessa raschii* and *Meganyctiphanes norvegica*) in the lower estuary and Gulf of St. Lawrence. Prog Oceanogr 131:159–176

Meyer-Gutbrod E, Greene C, Davies K, Johns D (2021) Ocean regime shift is driving collapse of the North Atlantic right whale population. Oceanog 34:22–31

Meyer-Gutbrod EL, Davies KTA, Johnson CL, Plourde S and others (2022) Redefining North Atlantic right whale habitat-use patterns under climate change. Limnol Oceanogr 68:577–586

Michaud J, Taggart CT (2011) Spatial variation in right whale food, *Calanus finmarchicus*, in the Bay of Fundy. Endang Species Res 15:179–194

Mitchell MR, Harrison G, Pauley K, Gagné A, Maillet G, Strain P (2002) Atlantic zonal monitoring program sampling protocol. Can Tech Rep Hydrogr Ocean Sci 223

Monsarrat S, Pennino MG, Smith TD, Reeves RR, Umr C (2015) Historical summer distribution of the endangered North Atlantic right whale (*Eubalaena glacialis*): a hypothesis based on environmental preferences of a congeneric species. Biodivers Res 21:925–937

Moore MJ, Rowles TK, Fauquier DA, Baker JD and others (2021) Assessing North Atlantic right whale health: threats, and development of tools critical for conservation of the species. Dis Aquat Org 143:205–226

Murison LD, Gaskin DE (1989) The distribution of right whales and zooplankton in the Bay of Fundy, Canada. Can J Zool 67:1411–1420

O'Brien O, Pendleton DE, Ganley LC, McKenna KR and others (2022) Repatriation of a historical North Atlantic right whale habitat during an era of rapid climate change. Sci Rep 12:12407

Parks SE, Warren JD, Stamieszkin K, Mayo CA, Wiley DN (2012) Dangerous dining: surface foraging of North Atlantic right whales increases risk of vessel collisions. Biol Lett 8:57–60

Payne R, Dorsey E (1983) Sexual dimorphism and aggressive use of callosities in right whales (*Eubalaena australis*). In: Payne R (ed) Communication and behavior of whales. Westview Press, Boulder, CO, p 295–329

Pedersen TL (2024) patchwork: the composer of plots. R package version 1.2.0.9000. https://github.com/thomasp85/patchwork

Pendleton DE, Pershing AJ, Brown MW, Mayo CA, Kenney RD, Record NR, Cole TVN (2009) Regional-scale mean copepod concentration indicates relative abundance of North Atlantic right whales. Mar Ecol Prog Ser 378: 211–225

Pettis HM, Pace RM, Hamilton PK (2021) North Atlantic Right Whale Consortium 2020 Annual Report Card. North Atlantic Right Whale Consortium. https://www.narwc.org/uploads/1/1/6/6/116623219/2020narwcreport_cardfinal.pdf

Plourde S, Runge JA (1993) Reproduction of the planktonic copepod *Calanus finmarchicus* in the lower St. Lawrence Estuary: relation to the cycle of phytoplankton production and evidence for a *Calanus* pump. Mar Ecol Prog Ser 102:217–227

Plourde S, Joly P, Runge JA, Dodson J, Zakardjian B (2003) Life cycle of *Calanus hyperboreus* in the lower St. Lawrence Estuary and its relationship to local environmental conditions. Mar Ecol Prog Ser 255:219–233

Plourde S, Lehoux C, Johnson CL, Perrin G, Lesage V (2019) North Atlantic right whale (*Eubalaena glacialis*) and its food: (I) a spatial climatology of *Calanus* biomass and potential foraging habitats in Canadian waters. J Plankton Res 41:667–685

R Core Team (2020) R: a language and environment for statistical computing. R Foundation for Statistical Computing, Vienna

Record N, Runge J, Pendleton D, Balch W and others (2019) Rapid climate-driven circulation changes threaten conservation of Endangered North Atlantic right whales. Oceanography 32:162–169

Rolland RM, Parks SE, Hunt KE, Castellote M and others (2012) Evidence that ship noise increases stress in right whales. Proc R Soc B 279:2363–2368

Sainmont J, Andersen KH, Varpe Ø, Visser AW (2014) Capital versus income breeding in a seasonal environment. Am Nat 184:466–476

Sheng J (2001) Dynamics of a buoyancy-driven coastal jet: The Gaspé Current. J Phys Oceanogr 31:3146–3162

Simard Y, Roy N, Giard S, Aulanier F (2019) North Atlantic right whale shift to the Gulf of St. Lawrence in 2015, revealed by long-term passive acoustics. Endang Species Res 40:271–284

Sobana M (2021) Energy content and biomass analysis of bulk mesozooplankton collected in the southern Gulf of St. Lawrence. BSc (Hon) thesis, University of New Brunswick, Saint John

Sorochan KA, Plourde S, Morse R, Pepin P, Runge J, Thompson C, Johnson CL (2019) North Atlantic right whale (*Eubalaena glacialis*) and its food: (II) interannual variations in biomass of *Calanus* spp. on western North Atlantic shelves. J Plankton Res 41:687–708

Sorochan KA, Brennan CE, Plourde S, Johnson CL (2021a) Spatial variation and transport of abundant copepod taxa in the southern Gulf of St. Lawrence in autumn. J Plankton Res 43:908–926

Sorochan KA, Plourde S, Baumgartner MF, Johnson CL (2021b) Availability, supply, and aggregation of prey (*Calanus* spp.) in foraging areas of the North Atlantic right whale (*Eubalaena glacialis*). ICES J Mar Sci 78: 3498–3520

Sorochan KA, Plourde S, Johnson CL (2023) Near-bottom aggregations of *Calanus* spp. copepods in the southern Gulf of St. Lawrence in summer: significance for North Atlantic right whale foraging. ICES J Mar Sci 80: 787–802

Stewart JD, Durban JW, Knowlton AR, Lynn MS and others (2021) Decreasing body lengths in North Atlantic right whales. Curr Biol 31:3174–3179

Stewart JD, Durban JW, Europe H, Fearnbach H and others (2022) Larger females have more calves: influence of maternal body length on fecundity in North Atlantic right whales. Mar Ecol Prog Ser 689:179–189

Suthers IM, Taggart CT, Rissik D, Baird ME (2006) Day and night ichthyoplankton assemblages and zooplankton biomass size spectrum in a deep ocean island wake. Mar Ecol Prog Ser 322:225–238

van der Hoop J, Corkeron P, Moore M (2017) Entanglement is a costly life-history stage in large whales. Ecol Evol 7: 92–106

van der Hoop JM, Nousek-McGregor AE, Nowacek DP, Parks SE, Tyack P, Madsen PT (2019) Foraging rates of ram-filtering North Atlantic right whales. Funct Ecol 33: 1290–1306

Watkins WA, Schevill WE (1976) Right whale feeding and baleen rattle. J Mammal 57:58–66

Wickham H (2016) Ggplot2: elegant graphics for data analysis. Springer-Verlag, New York, NY

Wickham H, Averick M, Bryan J, Chang W and others (2019) Welcome to the tidyverse. J Open Source Softw 4:1686

Woodley TH, Gaskin DE (1996) Environmental characteristics of North Atlantic right and fin whale habitat in the lower Bay of Fundy, Canada. Can J Zool 74:75–84

Editorial responsibility: Sascha Hooker, St. Andrews, UK
Reviewed by: 3 anonymous referees
Submitted: March 11, 2024; Accepted: September 2, 2025
Proofs received from author(s): November 25, 2025